

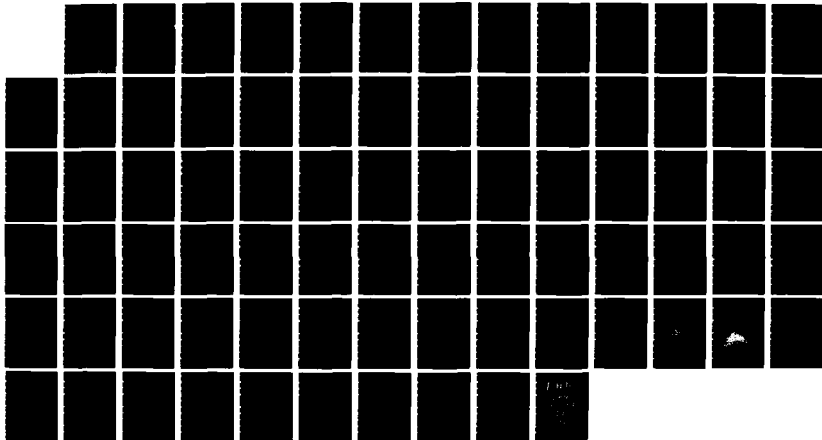
AD-A186 276

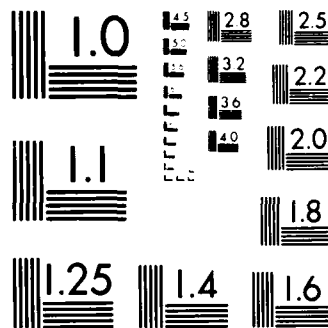
CARBON MONOXIDE AND TURBULENCE-CHEMISTRY INTERACTIONS:
BLOWOFF AND EXTINC (U) GENERAL ELECTRIC CO SCHENECTADY
N Y RESEARCH AND DEVELOPMENT C S M CORREA ET AL
31 MAY 87 AFOSR-TR-87-1162 F49620-85-C-0035 F/G 7/4

1/1

UNCLASSIFIED

NL





MICROCOPY RESOLUTION TEST CHART
NATIONAL BUREAU OF STANDARDS-1963-A

2

AD-A186 276

REPORT DOCUMENTATION PAGE

DTIC FILE COPY

Unclassified		10. RESTRICTIVE MARKINGS None	
2a. SECURITY CLASSIFICATION AUTHORITY		3. DISTRIBUTION/AVAILABILITY OF REPORT Distribution unlimited; approval for public release	
2b. DECLASSIFICATION/DOWNGRADING SCHEDULE			
4. PERFORMING ORGANIZATION REPORT NUMBER(S)		5. MONITORING ORGANIZATION REPORT NUMBER(S) AFOSR-TR- 87 - 1162	
6a. NAME OF PERFORMING ORGANIZATION General Electric Research and Development Center		7a. NAME OF MONITORING ORGANIZATION Air Force Office of Scientific Research	
6b. OFFICE SYMBOL (If applicable)		7b. ADDRESS (City, State and ZIP Code) Bolling AFB DC 20332-6448	
6c. ADDRESS (City, State and ZIP Code) PO Box 8 Schenectady, NY 12301			
8a. NAME OF FUNDING/SPONSORING ORGANIZATION Air Force Office of Sci. Res.		9. PROCUREMENT INSTRUMENT IDENTIFICATION NUMBER F49620-85-C-0035	
8b. OFFICE SYMBOL (If applicable) AFOSR/NA			
8c. ADDRESS (City, State and ZIP Code) Bolling AFB DC 20332-6448		10. SOURCE OF FUNDING NOS.	
		PROGRAM ELEMENT NO. PROJECT NO. TASK NO. WORK UNIT NO.	
		61162 2302 72	
11. TITLE (Include Security Classification) Carbon Monoxide and Turbulence-Chemistry Interactions: Blowoff & Extinction of Turbulent Diffusion Flames			
12. PERSONAL AUTHOR(S) Drs. S.M. Correa and A. Gulati			
13a. TYPE OF REPORT Annual report		13b. TIME COVERED FROM 1 June 86 to May 87	
14. DATE OF REPORT (Yr., Mo., Day) 1987, May, 31		15. PAGE COUNT 51 + figures & tables	
16. SUPPLEMENTARY NOTATION			
17. COSATI CODES			
FIELD GROUP SUB GR.			
18. SUBJECT TERMS (Continue on reverse if necessary and identify by block number) Turbulence-Chemistry interactions, extinction, blowoff, turbulent diffusion flames, superequilibrium, laser diagnostics			
19. ABSTRACT (Continue on reverse if necessary and identify by block number) <p>The goal of this program is to understand turbulence-chemistry interactions in combustion up to and including localized extinction. Experimentally, pilot-stabilized non-premixed turbulent jet flames of selected $\text{CO}/\text{H}_2/\text{N}_2$ mixtures are being studied under conditions conducive to strain-induced local extinction. Laser-based techniques such as Raman scattering and Rayleigh scattering are employed. Analytically, models based on the asymptotically-thin flamelet concept and on distributed reaction zone concepts are being assessed. A significant finding is that the popular contemporary view of a turbulent flame as an ensemble of asymptotically-thin flamelets seems incorrect. Alternative mechanisms based on "thick flamelets" are proposed.</p> <p style="text-align: right;">/cont'd over</p>			
20. DISTRIBUTION/AVAILABILITY OF ABSTRACT UNCLASSIFIED/UNLIMITED <input checked="" type="checkbox"/> SAME AS RPT <input type="checkbox"/> DTIC USERS <input type="checkbox"/>		21. ABSTRACT SECURITY CLASSIFICATION Unclassified	
22a. NAME OF RESPONSIBLE INDIVIDUAL Julian M. Tishkoff		22b. TELEPHONE NUMBER (Include Area Code) (202) 767-4935	
		22c. OFFICE SYMBOL AFOSR/NA	

19. cont'd

The results of the second year of this program include: (1) A complete re-evaluation of Raman data previously taken in an $Re=8500$ turbulent nonpremixed syngas flame, showing significant corrections due to high-temperature effects, (2) a detailed comparison with Monte-Carlo/partial-equilibrium calculations, bolstering the concept of partially-equilibrated radical pools in turbulent combustion, (3) the development of $CO/H_2/N_2$ mixtures with low extinction limits (approaching hydrocarbons) with Rayleigh-scattering cross-sections matched for density and with viability for Raman measurements, (4) a broad range of improvements to minimize interference due to chemi-luminescence in Raman measurements, (5) the design and construction of a co-annular premixed pilot for the nonpremixed burner, (6) detailed Raman measurements at $Re=5000$ and $Re=15,000$ in highly-strained regions as well as further downstream in the new pilot-stabilized flame, (7) comparison with a strained flamelet theory for localized extinction and, (8) the development of a theory which recognizes that a wide range of Damkohler numbers exists and so treats only fast reactions in the context of flamelets. The latter theory draws from earlier work on partial-equilibrium. Taken together, these results are a step towards understanding the nature of localized turbulent extinction, a precursor of blowout in practical devices under some conditions. In particular, the popular notion of thin flamelets as described by high-energy asymptotics is in serious difficulty, because of the wide spectrum of Damkohler numbers associated with the multi-step nature of chemical kinetics of combustion.

TABLE OF CONTENTS

Page

1. Summary	2
2. Research Objectives	3
3. Status	
3.1 Introduction	4
3.2 Turbulent Flame Facility: Summary of previous work	6
3.3 Re-analysis of Prior Data and Comparison with Model	9
3.4 High Reynolds Number Flame: Selection of Fuel	19
3.5 Pilot-Stabilized Burner	23
3.6 Improvements in Raman System	25
3.7 Experimental Results	27
3.8 Laminar Flamelet Model: Predictions and Comparison	30
3.9 Alternate Approach to Modeling Turbulent Extinction	39
3.10 Future Work	42

4. Publications and Presentations Supported by AFOSR Contract	43
---	----

5. Professional Personnel	44
---------------------------	----

References

List of Tables

Figure Captions

Accession For	
NTIS GRA&I	<input checked="" type="checkbox"/>
DTIC TAB	<input checked="" type="checkbox"/>
Unannounced	<input type="checkbox"/>
Justification	
By _____	
Distribution/ _____	
Availability Codes	
Dist	Avail and/or Special
A-1	



1. SUMMARY

The results of the second year of this program include: (1) A complete re-evaluation of Raman data previously taken in an $Re=8500$ turbulent nonpremixed syngas flame, showing significant corrections due to high-temperature effects, (2) a detailed comparison with Monte-Carlo/partial-equilibrium calculations, bolstering the concept of partially-equilibrated radical pools in turbulent combustion, (3) the development of $CO/H_2/N_2$ mixtures with low extinction limits (approaching hydrocarbons) with Rayleigh-scattering cross-sections matched for density and with viability for Raman measurements, (4) a broad range of improvements to minimize interference due to chemi-luminescence in Raman measurements, (5) the design and construction of a co-annular premixed pilot for the nonpremixed burner, (6) detailed Raman measurements at $Re=5000$ and $Re=15,000$ in highly-strained regions as well as further downstream in the new pilot-stabilized flame, (7) comparison with a strained flamelet theory for localized extinction and, (8) the development of a theory which recognizes that a wide range of Damkohler numbers exists and so treats only fast reactions in the context of flamelets. The latter theory draws from earlier work on partial-equilibrium. Taken together, these results are a step towards understanding the nature of localized turbulent extinction, a precursor of blowout in practical devices under some conditions. In particular, the popular notion of thin flamelets as described by high-energy asymptotics is in serious difficulty, because of the wide spectrum of Damkohler numbers associated with the multi-step nature of chemical kinetics of combustion.

2. RESEARCH OBJECTIVES

The research objectives of this program are to:

- A. Improve and expand the database for turbulent carbon monoxide/hydrogen/nitrogen jet flames utilizing pulsed Raman spectroscopic measurements.
- B. Use experimental results to evaluate assumptions made in formulating prediction methods based on probability density functions and on laminar flamelets.
- C. Modify the experimental facility to conduct turbulent jet combustion tests at Reynolds numbers greater than 9,000 without blow-off at nozzle. Use PLIF to visualize extent of extinction.
- D. Model a carbon monoxide/hydrogen/nitrogen jet flame at 8,500 Reynolds number using two-scalar and flamelet approaches.
- E. Conduct experiments on two carbon monoxide/hydrogen/nitrogen jet flames at Reynolds numbers above 9,000 under conditions of local extinction.
- F. Formulate alternatives to the partial-equilibrium chemical kinetics model previously used to predict the chemistry of carbon monoxide flames.

3. STATUS

3.1 Introduction

Development of a fundamental understanding of turbulence-chemistry interactions is one of the most important and challenging problems in turbulent combustion. Although the fast chemistry or "mixed-is-burned" model for combustion is useful for understanding gross aerodynamics in many combustion systems, there is an increasingly important range of phenomena that cannot be so accounted for. For example, finite-rate radical pool chemistry has been shown to be very influential in thermal NO_x and CO emissions from atmospheric H_2 and CO/ H_2 flames [Drake et al. (1987)] and to degrade combustion efficiency in supersonic combustion systems [Correa and Mani (1987)]. Localized effects including extinction due to turbulent stretching may be largely due to the chemistry not being fast compared with the turbulent microscales [Masri and Bilger (1984)], as has been demonstrated in laminar CH_4 flames [Tsuji and Yamaoka (1970)]. High-altitude limitations on aircraft combustors are caused in part by slow kinetics due to the low densities. It is clear that as the limits of combustion equipment are expanded, it is more and more important to account for finite-rate chemical kinetics. On the other hand, detailed chemical kinetic mechanisms have been established only for the combustion of relatively simple fuels such as H_2 , CO/ H_2 and CH_4 [Warnatz (1981)]. The combustion of complex hydrocarbons of practical significance is usually represented by a semi-empirical first step to simple constituents such as CO and H_2 , with subsequent oxidation of the latter [Warnatz (1981)]. This may compromise the understanding of, for example, "prompt" NO_x which is formed via hydrocarbon fragments [Iverach et al. (1972)]; it also leaves only the relatively simple

fuels as candidates for fundamental work in turbulent flames, where the chemistry must be known a priori.

The approach of this joint experimental/computational program is to study turbulence-chemistry interactions in pilot-flame stabilized, turbulent, non-premixed jet ("diffusion") flames of H_2 and $CO/H_2/N_2$ fuels, where the turbulent fuel/air mixing and combustion chemistry are reasonably well known. (The turbulence is understood better than that in the recirculating flowfields characteristic of practical burners). Experimentally our unique combustor facilities and laser measurement techniques are providing time- and space-resolved pointwise measurements of probability density functions of temperature, major species concentrations, density and mixture fraction in the flow. Two-dimensional images of the density field using planar Rayleigh scattering will indicate the local stretch (instantaneous gradient of compositional scalar). Experimental results on stretched laminar opposed-flow diffusion flames are also available for comparison. Similar images of the OH field will indicate the extent of localized extinction. Computationally, the single-scalar fast chemistry model with assumed shaped pdf, joint pdf models for scalar and dissipation rate closed with the laminar flamelet model, [Williams (1974)] and two- or three-scalar non-equilibrium approaches using mixture fraction and reaction progress variables are being developed. Detailed experiment-model comparisons are being used to assess models and so to provide a more fundamental understanding of turbulence-chemistry interactions and extinction.

3.2 Turbulent Flame Facility: Summary of Previous Work

Laser diagnostic techniques for planar OH fluorescence, laser velocimetry, pulsed-Raman scattering, and laser-saturated OH fluorescence have been used in our laboratory to characterize turbulent jet-diffusion flames with H_2 and $CO/H_2/N_2$ fuels. The characteristics of the unstabilized combustor and the initial conditions for the flames have been discussed in detail [Correa et al. (1984), Lapp et al. (1983)]. The combustor consists of a 3.2 mm internal-diameter fuel tube centered axially in a 15-cm-square by 1-m long test section. The fuel velocity was controlled by calibrated critical flow orifices and the velocity of the surrounding co-flowing air stream by a servo-control on the exhaust fan. For the H_2 flames, the fuel jet had an initial average velocity of 285 m/s and is expected to have a turbulent pipe-flow profile corresponding to a cold-flow Reynolds number of 8500. The inlet air velocity was 12.5 m/s and was flat to within $\pm 2\%$. The axial pressure gradient (determined by 14 wall-pressure taps and by free-stream velocity measurements) was -51 Pa/m. For the $CO/H_2/N_2$ flame, the initial molar ratio of the fuel was approximately 40%CO/30% H_2 /30% N_2 with a small amount of CH_4 ($\sim 0.7\%$) sometimes added. The initial fuel and air velocities were 54.6 m/s and 2.4 m/s, respectively, and were chosen to match the Reynolds number (8500) and initial fuel-to-air velocity ratio (22.8) of the H_2 flame. The initial jet velocity profile was measured 1 mm from the nozzle exit, and the axial pressure gradient was -1.0 Pa/m.

The experimental measurements on the turbulent H_2 flames are summarized elsewhere, particularly in Drake et al. (1986). The data include qualitative and quantitative imaging (Schlieren, shadowgraph, and planar OH fluorescence),

instantaneous measurements of velocity (laser velocimetry); simultaneous measurements of temperature, density, individual major species concentrations, and mixture fraction (pulsed-Raman); and instantaneous measurements of OH concentrations (laser-saturated fluorescence). A collection of instantaneous measurements at a given flame location provide probability density functions (both conventional and Favre averaged). Analysis of those pdf's have permitted determination of intermittency and conditional moments [Pitz and Drake (1986)]. The first four moments of the mixture fraction pdf show remarkable similarity to the moments measured in turbulent nonreacting jet flows and indicate the presence of broad mixing zones [Drake et al. (1985)]. Comparison of the Raman data with thermodynamic and fluid mechanic models quantify the importance of preferential diffusion [Drake et al. (1982)] of H_2 and of radical superequilibrium [Drake et al. (1986)]. Superequilibrium was confirmed by direct measurements of OH concentrations using laser-saturated OH fluorescence with measured mean OH concentrations far above adiabatic equilibrium values close to the nozzle and near equilibrium values far downstream.

The experimental measurements in the turbulent $CO/H_2/N_2$ flame are summarized in Correa et al. (1984) and Drake (1985). The data include velocity, temperature, density, mixture fraction, and individual species concentrations as in the H_2 flame. In addition, probe sampling measurements of average value of NO and NO_x were obtained for the base fuel (for thermal NO_x), with small amounts of NH_3 added (for FBN conversion), and with small amounts of CH_4 added (for prompt NO_x).

Extensive comparisons with a partial-equilibrium model for the radical pool and k-s/assumed shape pdf model for turbulent flow were reported by

Correa et al. (1984); a more sophisticated theory was presented by Correa (1986a). These theories successfully predicted the high levels of super-equilibrium free radicals and were extended to thermal NO_x via the Zeldovich mechanism in Drake et al. (1987). Additionally Pope and Correa (1986) used partial-equilibrium and a Monte-Carlo/joint pdf flow simulation to show that, in the same flame, most major species were well predicted except for CO. This discrepancy has been found, as discussed below, to stem from errors in the reduction of the Raman data. In fact, the partial equilibrium model seems to be more accurate than concluded by Pope and Correa (1986). Correa et al. (1987) have presented these arguments in detail.

In the first year of the current program [Correa (1986b)] difficulties associated with measurement of CO_2 by Raman scattering were addressed, the laminar flamelet approach was assessed by examination of the Raman data for turbulent H_2 and $\text{CO}/\text{H}_2/\text{N}_2$ jet flames in coflowing air at Reynolds numbers of 8500 or less and a pilot-stabilized burner for high Reynolds number flames was designed. As a consequence of these studies, the CO_2 measurement in our Raman system is systematically improved; we also raised serious questions regarding the validity of viewing nonpremixed turbulent flames as ensembles of stretched laminar flamelets. The arguments will not be reproduced here.

Work performed in the second year follows along the same lines. New data and modeling in high Reynolds number nonpremixed turbulent flames are providing a basis for evaluating current ideas on turbulence-chemistry interactions including extinction and for formulating new approaches.

3.3 Reanalysis of Prior Data and Comparison with Model

A significant improvement in the analysis of the raw Raman data for the $Re = 8500$ flame of 40% CO , 30% H_2 , 30% N_2 fuel was made by correcting for the fraction of Raman signal in the Raman band pass of the major species (O_2 , N_2 , H_2 , H_2O , CO) at elevated temperatures. This correction factor was inadvertently set to unity in prior analyses of the raw Raman signals. The significance of this correction to the measured Raman signal at elevated temperatures arises from the fact that the Raman exit slits have a finite width due to space limitations and noise considerations; therefore significant portions of the hot Raman bands at higher temperatures do not fall within the finite exit slit and are not measured. The correction factors required to account for the limited Raman spectral band pass are a function of the species involved, temperature, width of the exit slit and the wavelength region covered by the physical Raman band pass. They were calculated by determining the fraction of the predicted Raman vibrational contour in the Raman bandpass using codes developed by Lapp et al. (1983). Table 1 lists typical values of the correction factors for the major species involved. As can be seen, the correction factors for H_2 and H_2O are significantly in excess of unity, whereas those for CO , O_2 and N_2 are less than unity. Table 2 compares typical mean values of temperature, mixture fraction and mole fractions of major species obtained at $x/d=25$ in the $Re=8500$ syngas flame for two cases (a) all correction factors set to unity and (b) correction factors allowed to assume proper values (listed in Table 1). The mean temperature values are less sensitive to non-unity correction factors since temperature is based upon the sum-of-mole-fraction method which is not significantly affected by the corrections.

However, the mole fractions of some major species including CO, H_2O and H_2 are found to differ by as much as 20%. The mixture fraction values, which are based on the hydrogen element are found to increase by 20% corresponding to the increase in the mole fractions of H_2 and H_2O .

Table (1)

High temperature correction factors for vibrational Raman scattering
used to correct for fraction of hot bands of various species falling
outside their respective exit slits.

Temp. (°K)	O ₂	CO	N ₂	H ₂ O	H ₂
300	1.00	1.00	1.00	1.000	1.000
600	.975	.994	1.019	1.001	1.014
900	.914	.966	1.009	1.011	1.060
1200	.848	.922	.982	1.058	1.133
1500	.799	.876	.953	1.141	1.229
1800	.769	.839	.932	1.270	1.345
2100	.756	.812	.922	1.440	1.479
2400	.757	.796	.922	1.650	1.629
2700	.768	.790	.932	1.900	1.795
3000	.787	.792	.950	2.159	1.976

Table (2a)

Temperature and mole fraction of major species at $x/d=25$ obtained without correcting for high temperature effects (correction factors set to unity).

(30% H_2 , 40% CO , 30% N_2) $Re = 8500$, $x/d = 25$

Position (x/a)	Temperature	Mole Fraction						Mixture Fraction	
	T/2000K	CO_2	O_2	CO	N_2	H_2O	H_2	Conv.	Favre
.63	.600	.084	.007	.233	.489	.105	.075	.443	.448
1.89	.687	.099	.012	.189	.530	.114	.049	.385	.39
3.15	.722	.110	.034	.127	.587	.109	.024	.297	.293
4.39	.647	.101	.084	.054	.655	.090	.008	.199	.176
5.66	.478	.061	.139	.021	.706	.062	.002	.117	.081
6.92	.333	.035	.175	.010	.733	.037	.001	.059	.033
8.18	.229	.017	.194	.004	.757	.019	.001	.023	.011
9.44	.159	.005	.208	.001	.770	.007	0.000	.004	.001
10.69	.146	.004	.209	.001	.772	.004	0.000	.001	.000

Table (2b)

Temperature and mole fraction of major species at $x/d=25$ corrected
for high temperature vibrational bands using the correction factors
listed in Table 1.

Position (x/a)	Temperature	Mole Fraction						Mixture Fraction	
	T/2000K	CO ₂	O ₂	CO	N ₂	H ₂ O	H ₂	Conv.	Favre
0.63	.638	.080	.005	.193	.505	.122	.090	.541	.541
1.89	.739	.093	.007	.144	.545	.141	.062	.504	.506
3.15	.785	.104	.025	.085	.605	.141	.032	.408	.396
4.39	.699	.096	.072	.025	.676	.113	.010	.267	.225
5.66	.504	.059	.129	.004	.725	.072	.003	.145	.093
6.92	.343	.034	.169	0.000	.746	.040	.001	.067	.036
8.18	.231	.016	.191	0.000	.763	.019	.001	.024	.011
9.44	.159	.005	.207	0.000	.771	.007	0.000	.004	.001
10.69	.146	.004	.209	0.000	.773	.004	0.000	.001	.000

The results of the partial-equilibrium/Monte-Carlo model [Pope and Correa (1986)] were compared with data on the non-premixed 40% CO, 30% H₂, 30% N₂ "syngas" jet flame in co-flowing air. The Raman data on major species density and temperature are those of Lapp et al. (1983) corrected here for high temperature effects as described above. The Raman data are compared at three axial locations, ($x/d=10, 25$ and 50); $x/d=50$ corresponds approximately to the visible length of the flame.

Radial profiles of the Favre-averaged mean mixture-fraction (ξ) agree quite well at $x/d=10$ (Fig. 1) except that the jet is predicted to have decayed too slowly on the centerline, and ξ is slightly overspread at the boundary. These differences are exaggerated in the mean density normalized by that of air (Fig. 1). The central region of the jet is hotter (lower density) than indicated by the data. Temperature profiles (Fig. 2) further confirm this discrepancy and also indicate a difference of about 100K in the off-axis peaks. Nitrogen concentrations plotted in Fig. 2 show better agreement. It should be recalled that the mixture fraction data are based on the measured H₂ and H₂O concentrations. More will be said on this below. Some of the other mean major species concentrations are shown in Fig. 3. Compared with the data, CO is underpredicted by 12% at worst, H₂ is overpredicted by about 10%, and CO₂ is overpredicted, which is consistent with a carbon balance. The jet spread is again slightly overpredicted. The discrepancies in the core seem consistent with overpredicting the amount of CO burned and therefore the temperature. The oxygen profiles also appear to agree reasonably well.

Mean mixture fraction and density at $x/d=25$ show that the jet spread is predicted quite well but the centerline mixture fraction is about 10% too low

(Fig. 4). Correspondingly, since the gas is predicted to be closer to stoichiometric, the temperature is higher by about 150°K than measured in the central region (Fig. 5). The spread rate appears quite reasonable. Once again, the nitrogen profiles (Fig. 5) agree well except in the central region, i.e., $r/a < 4$.

Mean major species concentrations at $x/d=25$ are shown in Fig. 6. The agreement is much better than presented in Pope and Correa (1986) because of the changes in the Raman data. Here CO is underpredicted by at worst 10% and O_2 , H_2 and CO_2 are predicted very well. In fact, the error in CO is rather more suggested of an over-diffusive calculation, although of course that is not inherent within the Monte-Carlo/joint pdf model, than a systematic error which might be attributed to a breakdown of partial-equilibrium in the radical-pool.

Mean mixture fraction profiles at $x/d=50$ show significant disagreement whereas the mean density (Fig. 7) agrees well with the data. Mean temperature and N_2 concentrations also agree fairly well as seen in Fig. 8. The good agreement in N_2 mole fraction is at first glance surprising given the relative lack of agreement in ξ . N_2 is essentially an inert species - only trace quantities are converted to NO_x - and therefore should follow a conserved scalar distribution.

This apparent contradiction can be resolved. The measurement of the mole fraction of N_2 is independent of the systematic errors involved in the measurement of other species, whereas the mixture fraction is a derived quantity which involves errors in measurements of all major species. The instan-

taneous value of fraction, ξ , can e.g. be defined as

$$\xi = \frac{X_{N_2} / (\sum X_i w_i)_{\text{mixture}} - X_{N_2}^{\text{air}} / w_{\text{air}}}{X_{N_2}^{\text{jet}} / w_{\text{jet}} - X_{N_2}^{\text{air}} / w_{\text{air}}} \quad (1)$$

Hence, the systematic errors in ξ are due to (a) errors in measurement of all major species and, (b) neglecting all radicals and other minor species since they are not measured by Raman scattering. These errors affect the "measured" molecular weight $\sum X_i w_i$ used in Eq. (1). In fact, a change in mean molecular weight of the gas mixture from 27.86 to 28.8, for the same measured mole fraction of Nitrogen ($X_{N_2}=0.711$) results in the mixture fraction changing from 0.15 to 0.22. Thus, "measurements" of the mixture-fraction are very sensitive to the molecular weight of the mixture especially at low values of ξ (as at $x/d=50$). It should be noted that all the data for ξ are based on Hydrogen element, but the same argument holds since, as Table 3 shows, the value of ξ based on three elements (C,H and N) agree well. This result is expected since the effects of differential diffusion, observed in flames at lower Reynolds numbers [Drake et al. (1982)] should be negligible in this (high Reynolds number) flame. Systematic errors in the measurement of ξ discussed above are common to the three cases.

Table (3)

Mean mixture fraction at $y=0$ obtained on the Carbon, Hydrogen and Nitrogen elements.

x/d	Based on N	Based on H	Based on C	Predicted Values
10	0.85	0.78	0.85	0.83
25	0.59	0.54	0.52	0.48
50	0.27	0.28	0.23	0.15

The comparison between data and the model predictions show that with the addition of two variables to describe the non-equilibrium kinetics and thermochemistry, it now appears that finite-rate radical pool kinetics can be predicted with reasonable accuracy in the context of turbulent non-premixed syngas flames. Results plotted here show better agreement with (re-analyzed) data on major species than previously thought. Thus, this study shows that the partial-equilibrium model for the oxyhydrogen radical pool including CO is more useful than was concluded by Correa (1986a) and Pope and Correa (1986). Although there are unresolved discrepancies between the predictions and the data, these are perhaps due to the difficulty of obtaining and interpreting Raman data to a greater extent than previously thought. The re-analyzed data do not show large amounts of CO present where H_2 is absent, which would have been a strong indication of the breakdown of partial equilibrium. Generally good agreement on the minor species (OH) in this flame obtained earlier [Correa et al. (1984)] further supports the partial-equilibrium model and emphasizes the importance of the relatively slow radical-recombination chemistry.

3.4 High Reynolds Number Flame: Selection of Fuel

One of the primary goals of this study is to obtain a better understanding of non-equilibrium chemistry effects in turbulent jet flames at high strain rates. Such flames may have regions of locally extinguished eddies embedded in the flame, which may be a precursor to flame lift-off and blow-off. The probability of finding large regions of local extinction in the flame is a strong function of the fuel being used. The choice of the fuel was primarily motivated by the desire to increase this probability. However, there were other considerations involved in the choice of the fuel, which are discussed below. The fuel chosen for detailed study consists of 10% H_2 , 40% CO and 50% N_2 (by volume) and is referred to as LHC (Low Hydrogen Content) gas hereafter. The prime considerations in the selection of the fuel were:

1. The probability of extinction in the turbulent flame should be sufficiently high to warrant detailed measurements. To estimate the probability of extinction, a simple experiment was conducted to estimate the value of the critical strain rate parameter ($a_c = 2 V/a$). A counter-flow diffusion flame burner of the type used by Tsuji and Yamaoka (1970) and described in Drake (1985) was used to estimate the value of a_c for various fuel compositions. The burner consists of a 5 cm diameter cylinder (5 cm long) with a 60° sector porous plug which is used to stabilize a flame 2-5 mm away from the surface of the porous burner. The burner is installed in the subsonic low turbulence variable-free-stream velocity tunnel such that the 60° sector is symmetric about the stagnation stream line. As the free-stream air velocity is increased, the flame is pushed closer to the burner surface and eventually blows off

abruptly at a critical strain rate, for which the characteristic mixing time τ_m evidently exceeds the characteristic reaction time τ_c .

Figure 9 shows a plot of a_c as a function of percent Hydrogen in the fuel which consists of 50% N_2 and the rest CO. In these measurements the fuel velocity ratio was held constant to avoid excessive heat loss from the flame when it is close to the burner. As can be seen in the Figure, the value of a_c increases from 400 s^{-1} corresponding to 2% H_2 to 1350 s^{-1} corresponding to 15% H_2 . The value of a_c is 950 s^{-1} for the LHC gas chosen for this study. This value is much lower than the estimate ($12,000\text{ s}^{-1}$) for Hydrogen and the estimate (greater than 2000 s^{-1}) for med BTU gas (40% CO, 30% H_2 , 30% N_2) and is of the order of a_c for methane flames ($\sim 400\text{ s}^{-1}$).

The probability of local extinction thus decreases very rapidly as the hydrogen content is increased. For pure hydrogen flame it is almost impossible to achieve extinction. Even though data presented by Dibble and Magre (1987) show existence of eddies that are lean mixtures of air-fuel and have very low temperatures, these eddies may be the result of large holes in the flame through which air has penetrated into the main jet and mixed with fuel without burning. In fact, that flame was visually unsteady. In hydrocarbon flames there is evidence of local extinction at relatively low strain rates (as suggested by the low value of a_c) but hydrocarbon flames have the complications of involving complex chemistry which is not well understood and of being extremely unamenable to Raman measurement due to fluorescence interferences [Dibble et al. (1987)]. These measurements of a_c indicate that for the LHC

gas chosen for this study the probability of extinction is fairly significant.

2. The fuel should have relatively simple chemistry. The finite rate chemistry effects of $H_2/CO/N_2$ flames are fairly well understood. Both H_2 and H_2/CO turbulent flames at low Reynolds numbers have been studied in detail in the past [Drake and Kollmann (1985)]. The study of H_2/CO flames is also important because most hydrocarbon fuels undergo pyrolysis and form H_2 and CO as intermediate constituents before burning.
3. The resulting flame should be amenable to Raman diagnostics. Even though it is advantageous to reduce the H_2 content of the fuel, it was found that for less than 10% H_2 content, the amount of CO had to be increased significantly to obtain a stable flame. Excessive amounts of CO present in the flame seriously interfere with Raman diagnostics due to chemi-luminescent interference from $CO+O \rightarrow CO_2$ reaction. This chemi-luminescence is fairly broad-banded and extends all the way to the far red. Even though flame luminescence can be subtracted on a shot-to-shot basis during Raman data collection, the change in the chemi-luminescence during the time interval can result in spurious Raman signals. Thus, it was necessary to reduce both the CO and H_2 content of the flame as much as possible by diluting it with Nitrogen. For Nitrogen dilution more than 50% a stable flame at high Reynolds number could not be obtained even with the aid of a pilot. The LHC flame at 15,000 Reynolds number was fairly stable with the premixed pilot. Thus, the Raman feasibility, the stability of the flame and the probability of localized extinction required a compromise in the choice of the fuel composition.

4. A final consideration regarding the choice of the fuel was the ability to use Rayleigh scattering to obtain 2D images of density in the flame by matching the Rayleigh cross-section of air, fuel and products. With a fuel composed of 10% H_2 , 40% CO, 25% N_2 , and 25% Ar it is estimated that the change in Rayleigh cross-section between the fuel, air and products is less than 7%. This is an important property of the modified LHC gas for the measurement of strain rate in the future.

3.5 Pilot-Stabilized Burner

The basic subsonic low-turbulence combustion tunnel has been described in detail elsewhere (Lapp et al. (1983)). The combustor has been used extensively for experimental studies of laminar, transitional and turbulent Hydrogen diffusion flames in the past. The combustor was redesigned and rebuilt to stabilize the high Reynolds number LHC flame by providing a coaxial premixed pilot. The premixed pilot burner is designed in a manner similar to that suggested by Starner and Bilger (1985). The turbulent jet diffusion flame is stabilized at the tip of a nozzle of diameter 3.18 mm by the co-annular premixed pilot flame. The flow rates are measured using critical flow orifices. Two flames at cold flow exit velocities of 25 m/s and 80 m/s corresponding to Reynolds numbers of 5000 and 15,000, respectively, were studied.

The high Reynolds number turbulent flame of LHC fuel ($Re=15,000$) provides a fluctuating strain field which can cause local extinction when some critical strain rate is exceeded locally. Extensive regions of such localized extinction can result in eventual liftoff or blowoff of the flame. The pilot-stabilized burner is designed to provide a stable flame in the region of large strain near the exit yet devoid of gross unsteady features. The pilot flame results in reduced initial strain rates and provides radicals resulting in the stabilization of the main flame. Further downstream the turbulence is fully developed and the strain rate is still high. Figure 10 shows a schematic of the burner exit. The pilot flame consists of a stoichiometric mixture of the main-jet fuel (10% H_2 , 40% CO, 50% N_2) and air which were mixed well upstream of the combustor exit. This fuel-air mixture ratio ($\xi_g=0.43$) results in the combustion products of the premixed flame having the same C/H/O ratios as the

main fuel when burned stoichiometrically and simplifies the modeling of the flowfield by retaining the two-stream feature. The premixed annular burner has an open area five times that of the main jet. A flame arrestor consisting of 18 holes of 1 mm diameter each is installed 4 mm upstream of the exit to anchor the premixed flame. The exit velocity of the premixed products is estimated to be 20 m/s based on an estimated post-flame temperature of 2000°K. The co-flowing air velocity in the tunnel was set at 5 m/s. Figure 11 shows a schematic of the flame identifying the various regions in the flame. The pilot flame, the main jet and the region of maximum strain rate where the flame is narrow are also identified in the figure.

The main jet flame at $Re = 15,000$ is approximately 50 diameters long (based on main jet diameter). The premixed pilot flame extends to about 5-6 diameters when lit without the main jet. It is estimated that the enthalpy content contributed by the pilot is less than 5% of that by the main jet due to its relatively low volumetric flow rate.

3.6 Improvements in Raman System

Due to the high CO content of the flame and the high Reynolds number, it was found that there was severe interference from chemi-luminescence of the flame (blue) in all channels of the Raman system including $N_2(AS)$, $N_2(S)$, O_2 , CO, CO_2 , H_2O and H_2 . The background flame-luminescence was as large as the associated Raman signals in most cases. For the Raman diagnostic system to acquire meaningful data, not only should the actual background levels be low, but the change in flame background over the integration period of the Raman signal should be low compared to the signal itself. The following major improvements were made in the Raman system to minimize the problems due to interference from flame luminescence.

1. Introduced a polarization filter in the collection optics. Since the Raman scattered light is polarized (98%) at the same polarization as the incident laser light, whereas the flame chemiluminescence is unpolarized, a factor-of-two-improvement in signal-to-noise ratio was achieved by the introduction of the polarization filter.
2. The laser was focussed tightly by using a smaller focal length lens. This enabled a reduction in the entrance slit size and a corresponding reduction in the flame chemi-luminescence without reducing the Raman signal.
3. By reducing the elapsed time between the collection of data and the firing of laser beam from 13 μsec to 8 μsec , the effect of change in flame background during Raman integration time on the Raman signal was minimized.

4. A new photomultiplier tube to monitor the Rayleigh scattering signal was introduced in the system. Since the N_2 channel is affected most by the luminosity of the flame, the temperature measurements using the Stokes-Anti-Stokes method are susceptible. Hence, Rayleigh scattering was used to obtain an independent measurement of temperature. The Rayleigh scattering intensity I_s is given by the following expression (Dibble and Hollenbach (1981)).

$$I_s = CIN\Omega l \left(\frac{d\sigma}{d\Omega} \right) \quad (2)$$

where, C is a calibration constant of the collection optics, I is the incident laser intensity, N the molecular number density, Ω the solid angle of the collection optics, σ is the Rayleigh scattering setting cross-section of the gas molecules and l the length of the laser beam segment imaged onto the detector. In a uniform pressure field, the above expression is simplified using the ideal gas law to the following form:

$$I_s = CIN\Omega \frac{PA}{RT} \left(\frac{d\sigma}{d\Omega} \right) = \frac{K}{T} \left(\frac{d\sigma}{d\Omega} \right)_{\text{eff}} \quad (3)$$

where K is a constant, P is the pressure, T is the temperature of the gas and R is the universal gas constant. The above expression shows that variations in Rayleigh scattering intensity result both from temperature variations and changes in scattering cross-section. However,

$$\left(\frac{d\sigma}{d\Omega} \right)_{\text{eff}} = \sum_i x_i \sigma_i$$

and hence $I_s = K \sum_i x_i \sigma_i$ which implies that the Rayleigh scattered intensity can be related to temperature directly in jet diffusion flames only if either additional information about the change in the Rayleigh cross-section of the

gas mixture is available or if the average Rayleigh cross-section is constant. In this flame the Raman scattering signals from the major species were used to obtain information about changes in the Rayleigh cross-section of the mixture and thus measure temperature in an iterative manner.

3.7 Experimental Results

Raman measurements of instantaneous temperature, mixture fraction and mole fractions of major species were obtained in two flames at $Re = 5,000$ and for the $Re = 15,000$. No pilot flame was used for $Re = 5,000$ flame. The temperature was measured using three methods (1) Stokes-Anti-Stokes method based on nitrogen, (2) sum of mole fractions of major species and (3) Rayleigh scattering as discussed earlier. Figure 12 shows a comparison between the mean centerline temperature in the $Re = 15,000$ flame obtained using the above three methods. The variation in the mean temperature obtained using the three methods is at most $100^\circ K$. The Rayleigh scattering channel corresponds to the best signal-to-noise ratio and is the most reliable measurement. The mixture fraction was obtained based on the carbon element using the following definition.

$$\xi = \left(\frac{X_{CO} + X_{CO_2}}{0.4} \right) \frac{20.73}{(\sum X_i w_i)_{\text{major species}}} \quad (4)$$

Figures 13, 14 and 15 show the scattergrams of temperature vs. mixture fraction at various locations in the two flames. Each data point in the figures represents an instantaneous simultaneous realization of temperature and mixture fraction (based on carbon element). Figure 13 is the scattergram at $x/d=10$, $r/a=1.6$ in the $Re=5000$ LHC flame ("a" refers to the radius of the

main jet; $a = 1.59$ mm). The solid line in the figure represents an adiabatic equilibrium (AE) calculation. As can be seen in the Figure, most of the data lies on the slightly fuel rich side of the curve and the scatter is minimal. The temperature variation from AE is less than 500°K at this location. The departures from equilibrium represent the effect of turbulence and measurement error. However, the departures from equilibrium are small and do not present evidence of extinction.

Figures 14 and 15 present data obtained in the high $Re=15,000$ flame at $x/d=10$, $r/a = 1.89$ and $x/d=60$, $r/a = 3.77$ locations respectively. These locations are representative of the regions of high strain rate and of completely-mixed equilibrium flow, respectively. Figure 14 shows an enormous amount of scatter in the data (2000 points) and large departures from equilibrium values. The mixture fractions lie in the range 0.3 to 0.6 and temperature departures from equilibrium in the range $400-1200^\circ\text{K}$. The data points having mixture fraction values near stoichiometric and significantly low temperatures may represent locally extinguished flamelets. Local extinction refers to a stoichiometric mixture of fuel and air which is unburnt or has been extinguished; however, the data indicates limited evidence of local extinction i.e., in approximately only 20% of the realizations. Figure 15 shows the scattergram at $x/d=40$ at which location the fuel and air are significantly mixed and the strain rates are significantly lower. As can be seen, most of the data lies along the fuel rich side of the AE curve and the departures from equilibrium are minimal even though there is significant scatter in the data. There is virtually no evidence at all of localized extinction at this axial location.

Detailed profiles of temperature and mole fractions of major species at centerline and various x/d locations in the $Re = 15,000$ flame are compared with model predictions in the next section.

3.8 Laminar Flamelet Model: Predictions and Comparison

Under the assumption that the laminar flame thickness is small compared with the turbulent (Kolmogorov, Batchelor) scales in the flow, the "laminar flamelet" analysis for non-premixed turbulent flames has been advanced, e.g., by Liew et al. (1981). In this model, the instantaneous composition of the turbulent flow is assumed to correspond to that in an undisturbed laminar diffusion flame at the prevailing value of mixture fraction. As the authors pointed out, this model is superior to chemical equilibrium models, particularly in fuel-rich hydrocarbon flames where CO levels are far from equilibrium. The flamelet model also offers an alternative to explicit multi-variable representations of the chemistry, such as performed by Janicka and Kollman (1979) and Bilger (1980) for turbulent H_2 diffusion flames and Correa et al. (1984) for CO/ H_2 flames. The undisturbed flamelet model has also been used in other analyses, eg., Faeth and Samulson (1985) for sooting flames and Razdan and Stevens (1985) for CO flames. Turbulent flames are hypothesized to consist of an ensemble of these laminar flamelets.

Numerical studies of the structure of laminar diffusion flames with full kinetics indicate a strong dependence on the strain-rate (Miller et al. 1984). A configuration often studied is the counterflow porous-cylinder burner as used by Tsuji and Yamaoka (1970). It is now established that as the strain rate $2V/a$ - where "V" is the oxidizer velocity and "a" the cylinder radius - is increased, the maximum temperature in the system decreases until an abrupt collapse to inert flow occurs, at some critical level of strain. The critical strain varies with fuel type ranging from $\sim 12,000 \text{ s}^{-1}$ for H_2 [David et al. (1987)] to $\sim 400 \text{ s}^{-1}$ for methane (Miller et al. 1984), and is

approximately 850 s^{-1} for the LHC gas chosen for this study.

The importance of the scalar dissipation rate to flame structure can be shown as follows. When the species conservation equation

$$\rho u_k \frac{\partial Y_i}{\partial x_k} = \frac{\partial}{\partial x_k} (D_i \frac{\partial Y_i}{\partial x_k}) + \dot{w}_i \quad (5)$$

is transformed to a mixture-fraction space, i.e., a coordinate perpendicular to surfaces of constant (elemental) composition, it becomes

$$D_i \left(\frac{\partial \xi}{\partial x_k} \right)^2 \frac{d^2 Y_i}{d\xi^2} = - \dot{w}_i \quad (6)$$

which shows that when the scalar dissipation $\chi = D_i \left(\frac{\partial \xi}{\partial x_k} \right)^2$ gets too large, the term denoting reaction $\frac{d^2 Y_i}{d\xi^2}$ is reduced and the flame can be extinguished.

The sensitivity of the laminar flamelet to strain implies that the instantaneous composition in a turbulent flame will depend on the local strain as well as mixture fraction. This has been accounted for by Liew et al. (1984), who showed that the joint pdf $P(\xi, X_{\max})$ would govern the instantaneous structure. In physical terms, the composition would correspond to that at the same mixture fraction in a laminar flame subjected to the same strain. In principle, a "library" of such strained flames could be generated computationally or experimentally; however, Liew et al. (1984) adopted the simpler approach of sampling the undisturbed flame (from experimental data) or inert flow, depending on X at the location of maximum temperature (X_{\max}) being less or more than an assumed quenching value of scalar dissipation, X_q . In highly turbulent flames where the local pdf of strain results in $\bar{X} > X_q$ much of the

time, the mean flow would then be strongly biased towards the inert flow. Local extinction would therefore be very significant.

The model used in this study follows Liew et. al. (1984) but assumes that equilibrium (frozen) flow exists instantaneously depending on whether the local scalar dissipation rate is less (more) than some critical value X_q . The value of X_q is critical to the model predictions and here the results are compared for a range of values of X_q .

The argument by which the local distribution of scalar dissipation rate is obtained follows Liew et al. (1984). Kolmogorov's hypothesis of a log-normal distribution is made with the mean \bar{X} given by

$$\bar{X} = c_{\frac{1}{2}} \zeta'^2 \bar{Z}/\bar{X} \quad (7)$$

which is the modelled term in the transport equation for the variance of mixture fraction. The local pdf for X is

$$P(X) = \frac{1}{X} \frac{1}{\sigma} \frac{1}{(2\pi)^{1/2}} \exp[-(\ln X - \mu)^2 / 2\sigma^2] \quad (8)$$

where σ^2 is the variance of $\ln X$. The pdf of X conditioned on the presence of zones of intense reaction (X_{max}), is assumed to be identical and may be integrated to give the probability of being below a critical level X_q , i.e., the probability of combustion P_c :

$$P_c = 1 - \frac{1}{2} \operatorname{erfc} \left[(\ln X_q - \mu) / \sqrt{2} \sigma \right] \quad (9)$$

As the gas flows downstream, the strain rates decrease and the probability P_c of the gas being below the burning limit increases. Thus, more of the gas is

equilibrated.

The pdf over thermochemical states is needed to obtain various quantities such as mean density. Since the flow is either inert (u) or in a state of equilibrium (e), the pdf is $P(\xi) = (1-P_c) P_u(\xi) + P_c \cdot P_e(\xi)$ where P_c is the fraction of gas which is burning. The pdf for the occurrence of values of the mixture fraction is needed. Such pdf's can be obtained directly from evolution equations based on the Navier-Stokes and species equations [Pope (1981)] or more simply by assumed-shape pdf methods as in Kent and Bilger (1976) for $P(\xi)$.

The pdf is widely adopted as being a beta-function

$$P(\xi) = \beta(\xi) \quad (10)$$

which can be parameterized in terms of its lowest moments, i.e., the mean and variance, and so varies throughout the flowfield.

The computational procedure may be summarized as follows: The shear-layer equations

$$\frac{\partial}{\partial x} (\rho u \phi_i) + \frac{1}{r} \frac{\partial}{\partial r} (r \rho v \phi_i) = \frac{1}{r} \frac{\partial}{\partial r} (r \Gamma_i \frac{\partial \phi_i}{\partial r}) + s_i \quad (11)$$

are solved in x-stream function coordinates using the numerical technique of Patankar and Spalding (1972). Here ϕ_i is, respectively, the axial velocity, turbulence kinetic energy, dissipation rate, and mean and variance of mixture fraction. The source term S_i and the transport coefficient Γ_i are chosen appropriately for particular equation. Inlet and boundary conditions on the variables correspond to fully-developed turbulent fuel flow with an assumed

intensity and length-scale of turbulence. The flow exiting the annulus is assumed to be completely burned.

At each point in the flow the local properties are obtained by weighting between the inert and burning flow properties with the probability of combustion, P_c , obtained from Eqs. (8). The properties of the burning gas are obtained by convoluting the local pdf $P(\xi, \vec{x})$ from Eqs. (10) with the corresponding thermochemical properties, such as $T(\xi)$ or $\rho(\xi, \eta)$, from the equilibrium combustion model.

Figure 16 shows the centerline axial variation of mean temperature. The model predictions for $X_q = 40, 100$ and 1000 s^{-1} are also shown. The experimental data follows a similar trend though the model predicts a slower growth rate for all values of X_q . The deviations of predictions from data are greatest at $x/d = 20$. Further downstream (e.g., at $x/d = 50$) the strain rates are expected to be much lower and so the predicted profiles for all these values of X_q collapse and are much closer to the experimental results. This however, is not conclusive support of the model because if a flamelet is quenched in the large strain region (lower x/d values) then it is premixed and cannot be described adequately by the model. This is because the model is applicable to strained flames of the diffusion type only whereas extinguished flamelets lead to a premixed situation.

Radial profiles of the modelled scalar dissipation rate for $X_q = 40, 100$ and 1000 at the axial location $x/d = 20$ (Figure 17) show large differences. This is because the jet is closer to equilibrium at the higher X_q which changes the penetration and mixing. These differences are reflected in signi-

ficant variations of the probability of combustion, i.e., the expectation \bar{X}_Q (Figure 18). Although it is not at present possible to measure the dissipation rate - which strictly-speaking would require measuring the mixture fraction in three dimensions with sufficient spatial and temporal resolution to resolve the smallest eddies - the scattergrams of temperature vs. mixture fraction in the zone of greatest strain indicate approximately a 20% probability of local extinction, as discussed above (Figure 15). This is of the same magnitude as the probabilities in Figure 18 for $\bar{X}_Q = 100$. The region of maximum probability of extinction and the trend of its radial variation are predicted well by the model.

Figures 19-21 show the density-weighted mean mixture fraction, conventional means of density and temperature at $x/d=20$. The jet spreads less rapidly than predicted by the model as seen by the narrower profile of mixture-fraction (Figure 19) and the centerline profile of mixture fraction (not shown). Differences in these profiles for different \bar{X}_Q are partially responsible for the differences in the mean density and temperature (Figures 20 and 21), but the latter differences are also due to the differing dissipation rates and probabilities of combustion. Thus the choice of \bar{X}_Q has a large influence on the results. From Figure 19 it appears that the best comparison is obtained for $\bar{X}_Q=1000$, but that implies an equilibrium flame and is in contradiction with the observations made in Figures 16 and 18. The agreement for $\bar{X}_Q=1000$ should be viewed as fortuitous and probably due to errors in the spread-rate due perhaps to mis-estimates of inlet conditions. Well downstream of the flame zone, the strain-rate is reduced and predictions become relatively insensitive to \bar{X}_Q . Figures 22-24 again compare predicted radial pro-

files of density-weighted mean mixture fraction and conventionally-averaged mean density and temperature with the Raman data. The probabilities of combustion tend to unity in all the cases - because the strain-rates are so low at this location. The predicted profiles are quite close to each other and to the data. The relatively good agreement with the data may be fortuitous because as discussed earlier, the model does not represent premixed laminar flamelets (which were earlier quenched in regions of high strain rates) adequately.

Discrepancies in the region of greatest strain near the nozzle exit may be due to one or more of several possible causes. Exit conditions in the nozzle and pilot are difficult to characterize and may exert a non-trivial influence on the near-exit region despite the large shear. These conditions include turbulence quantities and the heat loss in the pilot. From model calculations it was found that the results are sensitive to the temperature profile at the exit of the premixed pilot burner. At present experiments are being conducted to measure the temperature profiles at the exit of the pilot burner directly to provide the initial conditions.

These findings may be summarized as:

1. There is no firm evidence of local extinction (to frozen conditions) in the LHC gas $Re = 15,000$ flame even in the regions of largest strain. The model predicts the maximum probability of extinction to be 30% in this flame at $x/d=20$. Experimentally, it is observed that approximately 20% of data points have mixture fraction values close to stoichiometric but have significantly lower temperatures than adiabatic equilibrium.

These low temperature eddies could result from any of the following reasons: (a) they could represent eddies which were extinguished but are above 300°K due to mixing with surrounding hot products, (b) they could represent strained eddies with much lower temperatures (than AE) due to large non-equilibrium chemistry effects, (c) they could represent mixed eddies which are partially burned (i.e. they were extinguished due to large strains after initial ignition), (d) they could represent artifacts of Raman probe averaging (Raman probe volume is $200\mu \times 200\mu \times 650\mu$). Further work is needed to identify the exact nature of these data.

2. The theoretical predictions of the model show that the results are very sensitive to the assumed value of X_q , the quenching parameter, especially in the region of large strain and are also sensitive to the assumed velocity and temperature profiles at the exit of the pilot burner. In the next year of the program the exit velocity and temperature profiles near the tip of the combustor will be measured using laser velocimetry and Raman scattering.
3. Even though the model provides significant insight into the quenching and localized extinction phenomena in turbulent diffusion flames, there is significant disagreement between the data and calculations especially at $x/d=20$. The relatively better agreement at $x/d=50$ may be fortuitous. The model suffers from serious drawbacks of (a) relying on a relatively arbitrary quenching parameter X_q , (b) an inability to adequately describe flamelets after they are quenched (premixed strained flamelets), and (c) considering only two types of flamelets, equilibrium

and unstrained. This suggests a need to improve the chemistry-modeling and to combine partial-equilibrium models which have been very successful in the past with laminar flamelet models as discussed below.

3.9 Alternate Approach to Modeling Turbulent Extinction

An important shortcoming of the laminar flamelet analyses is that in practice laminar flames are not necessarily thin compared with turbulent scales. In H_2 and CO/H_2 flames, there are two distinct sets of scales associated with the chemistry, that corresponding to two-body chain-branching or propagating reactions and that corresponding to three-body recombination reactions. The large disparity between these scales has lead to partial-equilibrium models which assume the two-body reactions to be in equilibrium [Janicka and Kollman (1979), Bilger (1980), Correa et. al. (1984), Correa (1986a), Pope and Correa (1986)]. This disparity also implies that in intense turbulence the two-body reaction zones would remain comparatively thin while the three-body zones would overlap, leading to distributed reaction zones which are incompatible with the laminar flamelet hypotheses.

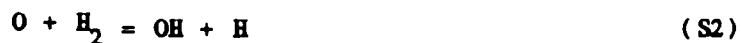
Thus, if independent control over the turbulent mixing was exercised, as the time-scale is progressively reduced from large values the OH (to pick a radical) would first increase as the recombination reactions are no longer fast enough to realize equilibrium, and then abruptly drop as the two-body reactions are quenched and the gas is inerted. Temperature shows a monotonic decrease throughout this process with a more rapid decrease as extinction is approached. This behavior is consistent with the notion that the abrupt transitions in a stretched flamelet are characteristic of high-activation energy (shuffle) reactions while well-distributed reaction zones are characteristic of low or zero activation-energy (recombination) reactions.

The large difference in the rates of the two-body and the three-body

reactions is apparent from experiments at relatively low Reynolds numbers. Correa et al. (1984) used the partial-equilibrium model for CO/H_2 in an $\text{Re} = 8500$ (cold jet) flame. The data indicated negligible or no local extinction - i.e., none of the Raman data showed low temperature in flammable gas - but large amounts of superequilibrium OH, up to factors of 5. The model agreed well with these data. One may conclude that the time-scales of turbulence in such flames are short enough to interfere with three-body recombination chemistry, i.e. a Damkohler number based on the recombination reactions is of $O(1)$. The time-scales are still too long to disturb the two-body reactions ($D_{2\text{-body}} \gg 1$) and so there is little or no local extinction.

Here it is proposed to retain the partial equilibrium model but with the quenched flamelet approach to the two-body reaction zone. The two-body reaction zone is assumed to be either in equilibrium or quenched (i.e., leading to inert flow) depending on the local strain \bar{X} being less or more than the quench level, X_q .

The kinetic mechanism adopted consists of five fast shuffle reactions (S1)-(S5), which are considered to be in partial equilibrium,



and the four relatively slow three-body recombination reactions (R1) - (R4)



First it must be recognized that the scalar dissipation rate continuously decreases as the fluid flows downstream. The region of intense stretch, which is visualized as being co-located with the 2-body shuffle reaction zone, therefore experiences a transition through the critical strain rate, and the 2-body reactions are assumed to immediately reach partial equilibrium. This is analogous to the approach used by Liew et al. (1984) who assumed a burnt flamelet state for the flamelets which were below a critical strain rate. In the present case only the 2-body reactions are assumed to reach equilibrium, the recombination reactions commence and drive the system towards full chemical equilibrium.

The concept is easily visualized as follows in one dimension. If the pdf's for scalar dissipation rate X at an upstream and downstream location are denoted by $P_u(X)$ and $P_d(X)$, respectively, and the probabilities of 2-body reaction equilibration are $P_u(X < X_{cr})$ and $P_d(X < X_{cr})$, then the probability that the recombination reactions "just" started is $P_d(X < X_{cr}) - P_u(X < X_{cr})$. The concept is currently being extended to multi-dimensional flow and will be used to replace the analysis of Section 3.8.

3.10 Future Work

For the next year of the program the following tasks have been identified:

1. Characterize the temperature and velocity profiles at the exit of the pilot combustor using Raman scattering and laser velocimetry.
2. Attempt to increase the probability of local extinction in the flame by further diluting the fuel with nitrogen and increasing the Reynolds number of the flame as much as possible.
3. Make Raman measurements in the H_2/CO flame to help identify the origin of the low temperature fuels-air eddies observed in the flame.
4. Obtain planar OH/Rayleigh images in the flame to determine flame connectivity/strain field at high Reynolds numbers.
5. Complete the modeling of the high Reynolds number plane using the joint partial equilibrium/flamelet type model discussed above and compare with experimental results.

4. PUBLICATIONS AND PRESENTATIONS SUPPORTED BY AFOSR CONTRACT

- A. Drake, M. C., (1986), "Stretched Laminar Flamelet Analysis of Turbulent H_2 and $CO/H_2/N_2$ Diffusion Flames," Twenty-first Symp. (Int.) on Combustion Munich, FRG.
- B. Drake, M. C. and Fenimore, C. P., (1986), "Stretched Laminar Opposed-Flow Diffusion Flame Experiments: Extinction and Nitric Oxide Formation," submitted for publication.
- C. Gulati, A. and Correa, S.M., (1987), "Local Extinction Due to Turbulence in Non-Premixed Flames," to be presented at AIAA/ASME/SAE 23rd Joint Propulsion Conference, June 23-July 2, San Diego, CA.
- D. Correa, S.M., Gulati, A. and Pope, S.B., (1987), "Assessment of a Partial-Equilibrium/Monte-Carlo Model for Turbulent Syngas Flames," Submitted for publication.

Related Publications and Presentations

- E. Correa, S. M., (1985), "Nitric Oxide Formation and Turbulent Flame Structure," Eastern States Section/Combustion Institute, Fall Technical Meeting, Philadelphia, PA.
- F. Pope, S. B. and Correa, S. M., (1986), "Joint Pdf Calculations of a Non-Equilibrium Turbulent Diffusion Flame," Twenty-first Symp. (Int.) on Combustion, Munich, FRG (1987).

G. -

5. PROFESSIONAL PERSONNEL

The following personnel contributed to this research:

- (i) Dr. A. Gulati
- (ii) Dr. S. M. Correa
- (iii) Mr. Frank Haller

REFERENCES

1. Bilger, R.W., (1980) Comb. Sci. Tech. 22, pp. 251-261.
2. S.M. Correa, M.C. Drake, R.W. Pitz, and W. Shyy, (1984) Twentieth Int. Combust. Symp., The Combustion Institute, 337.
3. Correa, S.M., (1986) "Carbon Monoxide and Turbulence-Chemistry Interactions: Measurements and Modeling of Turbulent Jet Diffusion flames," Annual Report, AFOSR Contract No. F49620-85-C-0035 (1986b).
4. Correa, S.M. and Mani, R., (1987) "A Non-Equilibrium Model for Hydrogen Combustion in Supersonic Flow," AIAA 23rd Joint Propulsion Conference, San Diego, CA.
5. Correa, S.M., Gulati, A., and Pope, S.B. (1987), "Assessment of a Partial-Equilibrium/Monte-Carlo Model for Turbulent Syngas Flames," submitted for publication.
6. Correa, S.M., (1986a), Arch. Comb., 5, No. 3-4, pp. 223-242.
7. David, T. P.H. Gaskell, and G. Dixon-Lewis, (1987), "Structure and Properties of Methane-Air and Hydrogen-Air Counterflow Diffusion Flames," submitted for publication.
8. R.W. Dibble, A. Masri, and R.W. Bilger, (1987), "The Spontaneous Raman Scattering Technique Applied to Nonpremixed Flames of Methane," Comb. and Flame, 67, 189. See also Figure 16 of Reference 5.

9. Dibble, R.W., and Magre, P., (1987) SANDIA Report 85-3601.
10. G. Dixon-Lewis, T. David, P.H. Gaskell, S. Fukutani, H. Jinno, J.A. Miller, R.J. Kee, M.D. Smooke, N. Peters, E. Effelsburg, J. Warantz, and F. Behrendt, Twentieth Int. Combust. Symp., The Combustion Institute, 1893, 1984.
11. M.C. Drake, R.W. Bilger, and S.H. Starner, Nineteenth Int. Combust. Symp., The Combustion Institute, Pittsburgh, 459, 1982.
12. M.C. Drake and W. Kollmann, (1985), "'Slow Chemistry Nonpremixed Flows,'" Evaluation of Data on Simple Turbulent Reacting Flows (W.C. Strahle, ed.), AFOSR TR-85 0880.
13. M.C. Drake, R.W. Pitz, and W. Shyy, (1985), "'Conserved Scalar PDFs in a Turbulent Jet Diffusion Flame,'" Turbulent Shear Flows V, 10.13.
14. Drake, M.C., R.W. Pitz, and J. Lapp, (1986), "'Laser Measurements on Nonpremixed Hydrogen-Air Flames for Assessment of Turbulent Combustion Models,'" AIAA J., 24, 6, 905.
15. Drake, M.C., Correa, S.M., Pitz, R.W., Shyy, W., and Fenimore, C.P., (1987), "Superequilibrium and Thermal Nitric Oxide Formation in Turbulent Diffusion flames," to appear in Combust. Flame.
16. Drake, M.C., Pitz, R.W., Correa, S.M. and Lapp, M., (1984a), Twentieth Symposium (International) on Combustion pp. 327-335.
17. Drake, M.C., "Kinetics of Nitric Oxide Formation in Laminar and Turbulent Methane Combustion," Report GRI-85/0271, Gas Research Institute,

Chicago, Illinois (1985).

18. G.M. Faeth and G.S. Samuelson, (1985), "'Fast Reaction Nonpremixed Combustion,'" Evaluation of Data on Simple Turbulent Reacting Flows (W.C. Strahle, ed.) AFOSR TR-85 0880.
19. Iverach, D., Hasden, K.S., and Kirov, N.Y., (1972), Fourteenth Symposium (International) on Combustion, The Combustion Institute, Pittsburgh, PA, pp. 767-775.
20. Janicka, J. and Kollman, W., Seventeenth Symposium (International) on Combustion, The Combustion Institute, Pittsburgh, PA., pp. 421-430. (1979).
21. Lapp, M., Drake, M.C., Penney, C.M., Pitz, R.W., and Correa, S.M., (1983), "Turbulent Combustion Experiments and Modeling," General Electric Report 83CRD049, DoE Contract DE-AC04-78 ET 13146.
22. S.K. Liew, K.M.C. Bray, and J.B. Moss, (1981), Combust. Sci. Tech. 27, 69.
23. S.K. Liew, K.M.C. Bray, and J.B. Moss, (1984), Combust. Flame 56, 199.
24. Masri, A.R. and Bilger, R.W., (1984), Twentieth Symposium (International) on Combustion, The Combustion Institute, Pittsburgh, PA, pp. 319-326.
25. J.A. Miller, R.J. Kee, M.D. Smooke, and J.F. Grcar, (1984), "'The Computation of the Structure and Extinction Limit of a Methane-Air Stagnation Point Diffusion Flame,'" Western States/CI Paper 84-20.

26. Patankar, S.V. and Spalding, D.B., (1972), Intertext Books, London.
27. R.W. Pitz and M.C. Drake, (1986), "'Intermittency and Conditional Averaging in a Turbulent Nonpremixed Flame by Raman Scattering,'" *ALAA J.*, 24, 5, 815.
28. Pope, S.B. and Correa, S.M., (1986), Twenty first Symposium (International) on Combustion, The Combustion Institute.
29. Pope, S.B., (1981), *Phys. Fluids*, 24, 4, pp. 588-596.
30. M.K. Razdan and J.G. Stevens, (1985), Combust. Flame 59, 289.
31. Tsuji, H., (1982), "Counter Flow Diffusion Flames," *Prog. Energy Combustion Science*, Vol. 8, pp. 93-119.
32. Tsuji, H. and Yamaoka, I., (1970), Thirteenth Symposium (International) on Combustion, The Combustion Institute, Pittsburgh, PA, pp. 723-731.
33. Varnatz, J., (1981), Eighteenth Symposium (International) on Combustion, The Combustion Institute, Pittsburgh, PA, pp. 369-384.
34. Williams, F.A., (1974), "'Recent Advances in Theoretical Descriptions of Turbulent Diffusion Flames,'" Turbulent Mixing in Nonreactive and Reactive Flows (S.N.P. Murthy, ed.), Plenum Press, 189.

List of Tables

1. High temperature correction factors for vibrational Raman scattering used to correct for fraction of hot bands of various species falling outside their respective exit slits.
- 2a. Temperature and mole fraction of major species at $x/d=25$ obtained without correcting for high temperature effects (correction factors set to unity).
- 2b. Temperature and mole fraction of major species at $x/d=25$ corrected for high temperature vibrational bands using the correction factors listed in Table 1.
3. Mean mixture fraction at $y=0$ obtained based on the Carbon, Hydrogen and Nitrogen elements.

List of Figures

- Fig. 1 Mixture fraction ξ and density $\bar{\rho}$ at $x/d=10$; $\xi \square, \bar{\rho} \circ$
- Fig. 2 Temperature \bar{T} and nitrogen mole-fraction \bar{X}_{N_2} at $x/d=10$; $\bar{T} \triangle, \bar{X}_{N_2} \circ$
- Fig. 3 Major species \bar{X}_i at $x/d=10$; $\bar{X}_{H_2} \circ, \bar{X}_{CO} \triangle, \bar{X}_{CO_2} \square, \bar{X}_{O_2} +$
- Fig. 4 Mixture fraction ξ and density $\bar{\rho}$ at $x/d=25$; $\xi \square, \bar{\rho} \circ$
- Fig. 5 Temperature \bar{T} and nitrogen mole-fraction \bar{X}_{N_2} at $x/d=25$; $\bar{T} \triangle, \bar{X}_{N_2} \circ$
- Fig. 6 Major species \bar{X}_i at $x/d=25$; $\circ \bar{X}_{H_2}, \triangle \bar{X}_{CO}, \square \bar{X}_{CO_2}, + \bar{X}_{O_2}$
- Fig. 7 Mixture fraction ξ and density $\bar{\rho}$ at $x/d=50$; $\xi \square, \bar{\rho} \circ$
- Fig. 8 Temperature \bar{T} and nitrogen mole-fraction \bar{X}_{N_2} at $x/d=50$; $\bar{T} \triangle, \bar{X}_{N_2} \circ$
- Fig. 9 Variation of α_c , the critical strain rate, with percent hydrogen in fuel (50% nitrogen, rest carbon monoxide).
- Fig. 10 Schematic of the burner exit.
- Fig. 11 Schematic of premixed pilot-stabilized burner showing the regions of maximum strain rates and fully developed turbulent-flame brush.
- Fig. 12 Centerline axial profile of mean temperature in $Re=15,000$ flame using these methods (a) SAS, (b) sum of mole species and (c) Rayleigh scattering.
- Fig. 13 Temperature vs. mixture fraction scattergram measured in the $Re = 5000$ flame at $x/d = 20$, $r/a = 2.52$ the solid line represents adiabatic equilibrium calculations for LHC gas in Figs. 13 through 15.
- Fig. 14 Measured temperature vs. mixture fraction scattergram in the $Re = 15,000$ LHC flame at $x/d = 10$, $r/a = 1.89$.
- Fig. 15 Measured temperature vs. mixture fraction scattergram in the $Re = 15,000$ LHC flame at $x/d = 40$, $r/a = 3.77$.

- Fig. 16 Axial variation of mean temperature at $y = 0$ in the $Re = 15,000$ LHC flame. Model predictions for X_q of 40,100 and 1000 s^{-1} are also shown in the figure.
- Fig. 17 Radial profile of predicted scalar dissipation rate of Liew et al. (1984). Stretched flamelet model at $x/d = 20$ for the values of $X_q = 40,100$ and 1000 .
- Fig. 18 Radial profile of predicted probability of combustion based on stretched flamelet model at $x/d = 20$ for three values of X_q .
- Fig. 19 Radial profile of measured Favre averaged mixture fraction at $x/d = 20$ compared with predictions of model for three values of X_q .
- Fig. 20 Radial profile of measured mean density at $x/d = 20$ compared with predictions of model.
- Fig. 21 Radial profile of measured mean temperature at $x/d = 20$ compared with predictions of model.
- Fig. 22 Radial profile of measured Favre averaged mixture fraction at $x/d = 50$ compared with predictions of model.
- Fig. 23 Radial profile of measured mean density at $x/d = 50$ compared with predictions of model.
- Fig. 24 Radial profile of measured mean temperature at $x/d = 50$ compared with predictions of model.

Fig. 1 Mixture fraction ξ and density $\bar{\rho}$ at $x/d=10$; ξ \square , $\bar{\rho}$ \circ

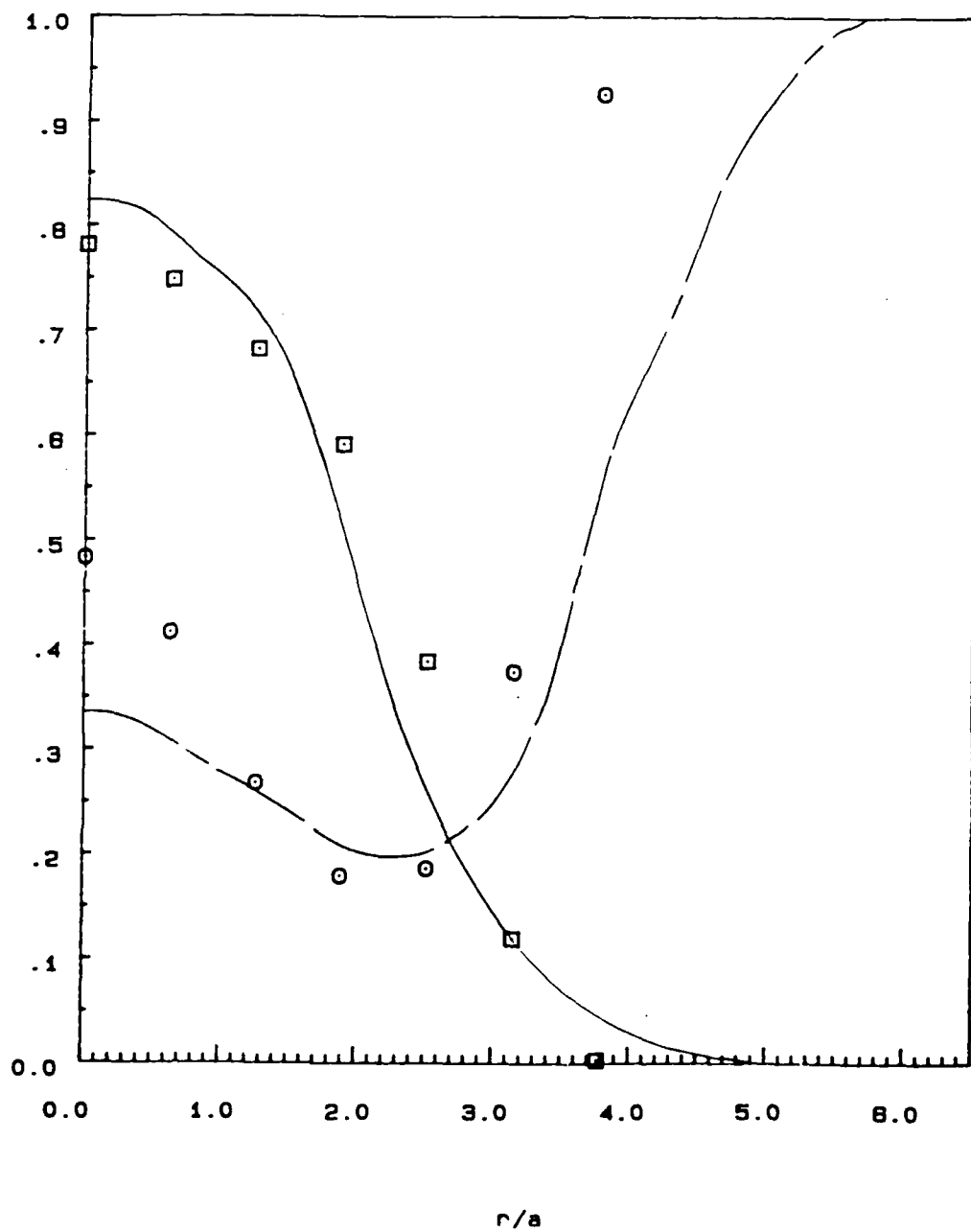


Fig. 2 Temperature \bar{T} and nitrogen mole-fraction \bar{X}_{N_2} at $x/d=10$;
 \bar{T} Δ , \bar{X}_{N_2} \circ

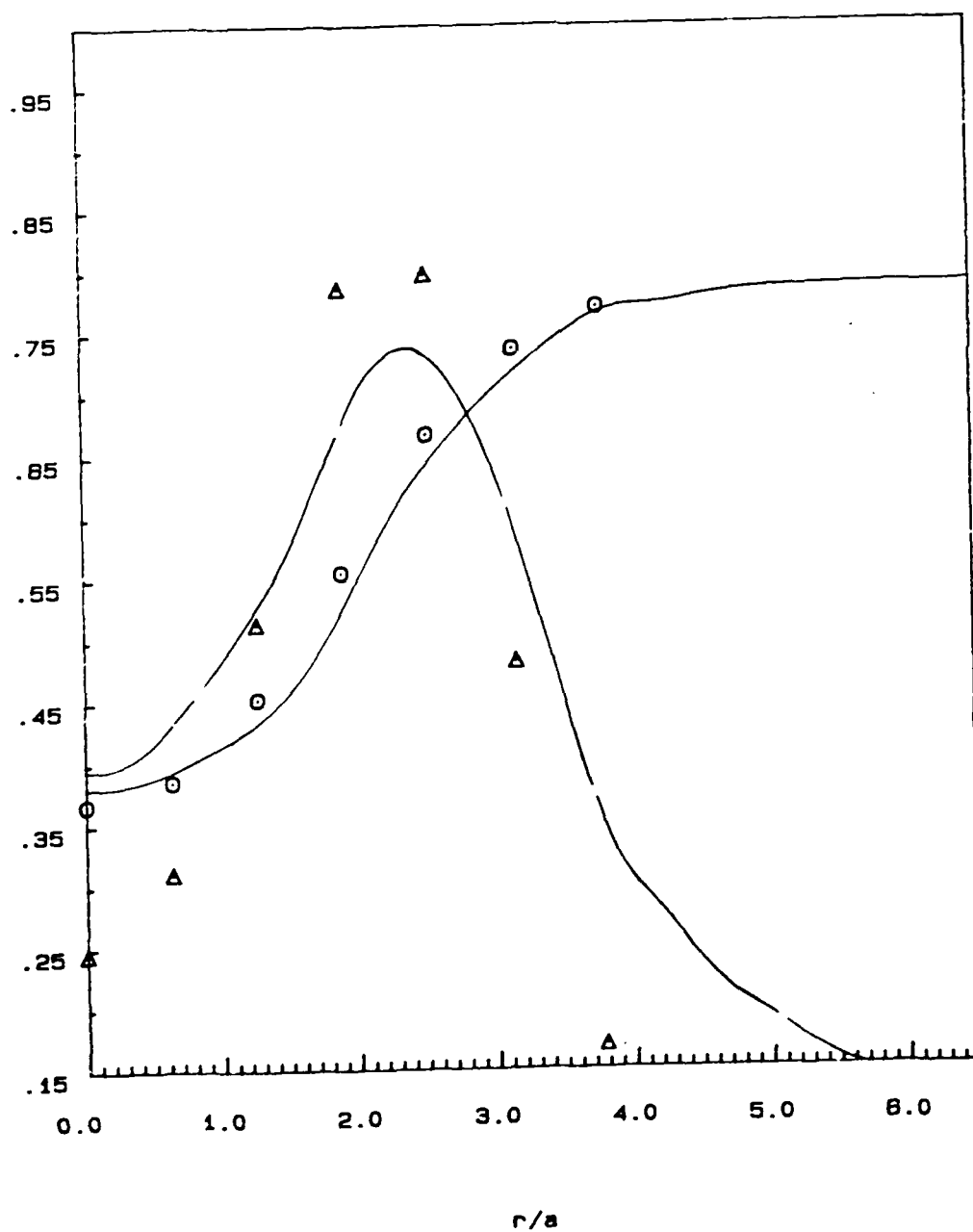


Fig. 3 Major species \bar{X}_i at $x/d=10$; \bar{X}_{H_2O} ○, \bar{X}_{CO} △, \bar{X}_{CO_2} □, \bar{X}_{O_2} +.

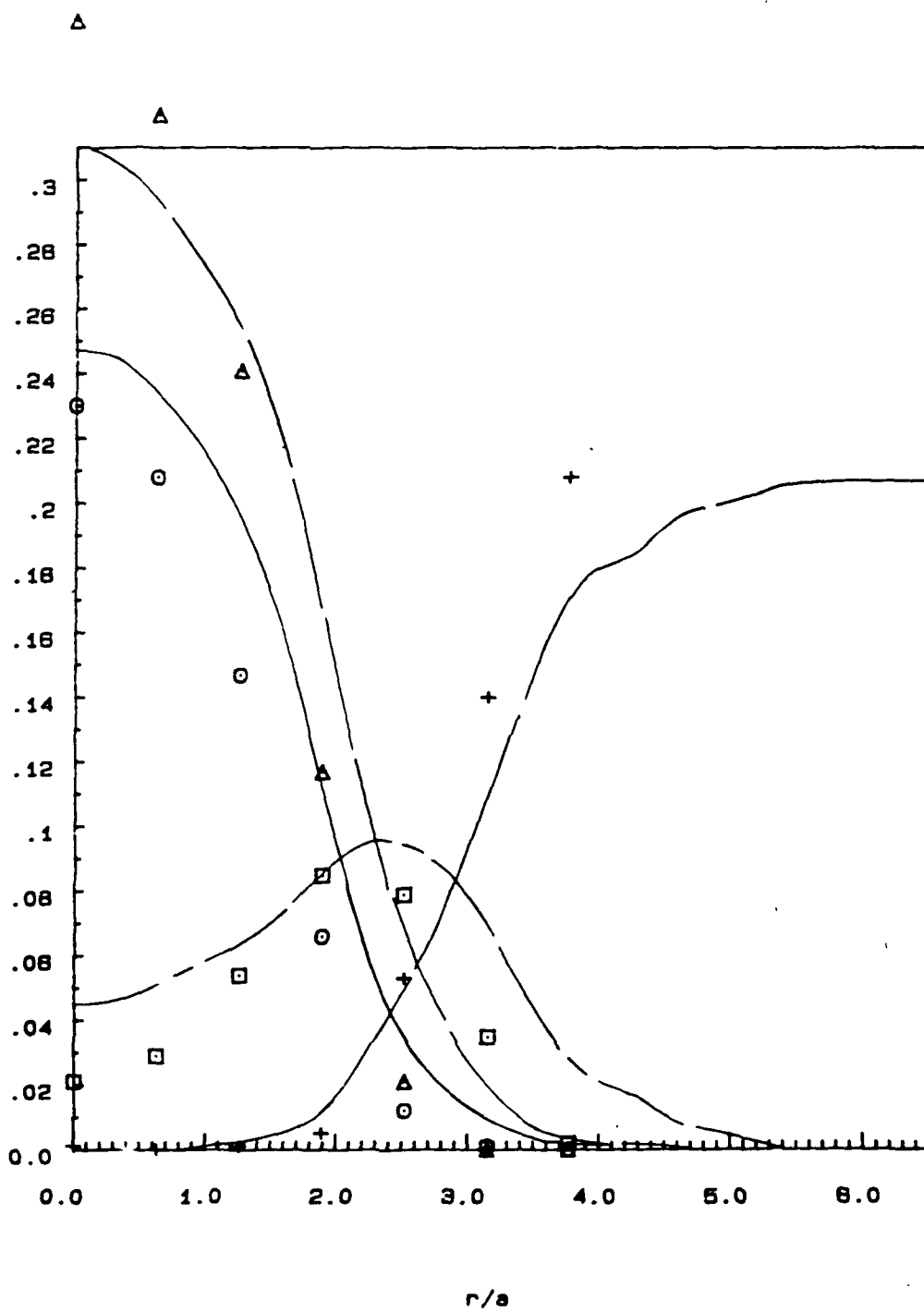


Fig. 4 Mixture fraction ξ and density $\bar{\rho}$ at $x/d=25$; ξ \square , $\bar{\rho}$ \circ

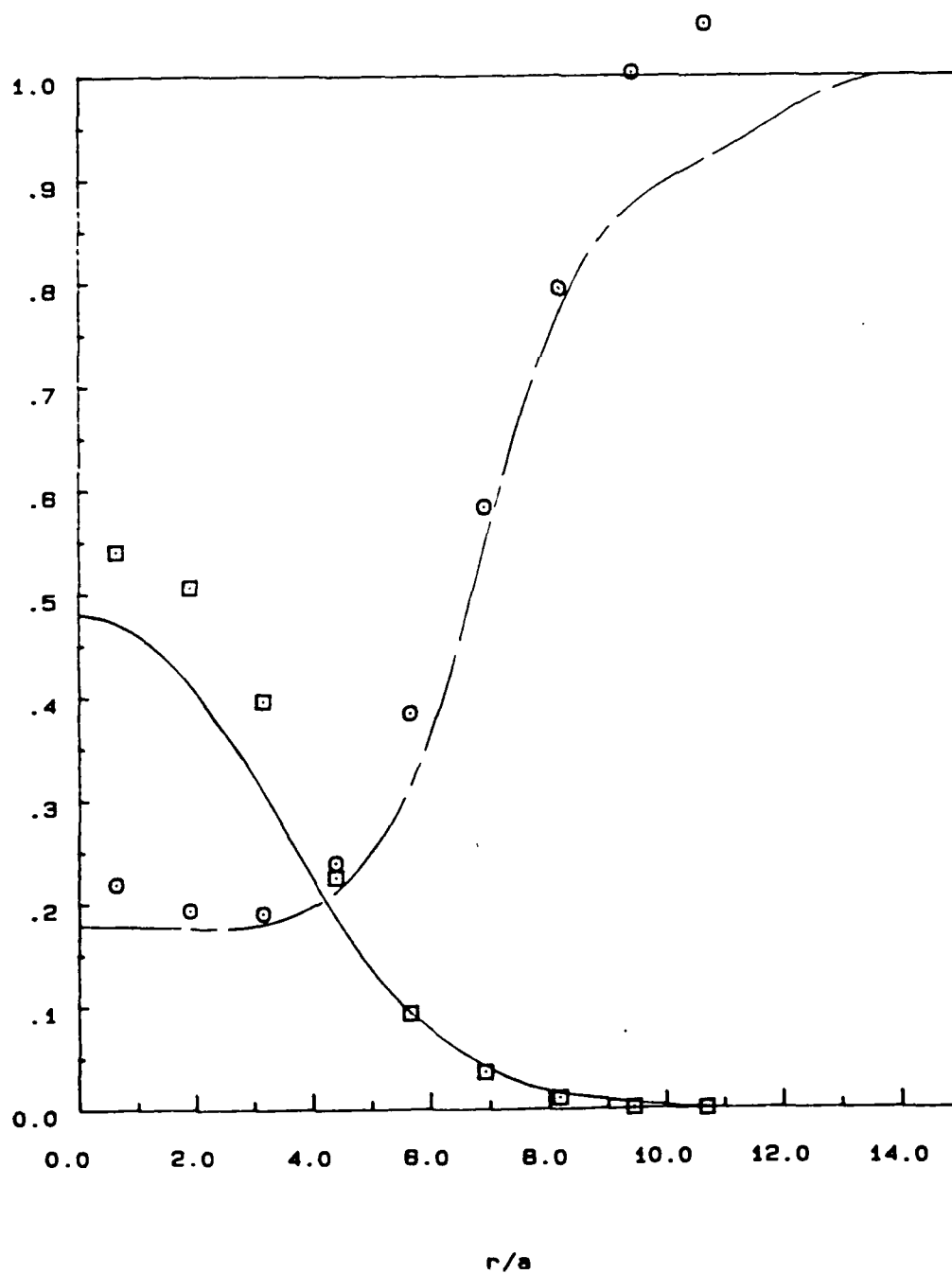


Fig. 5 Temperature \bar{T} and nitrogen mole-fraction \bar{X}_{N_2} at $x/d=25$; \bar{T} Δ , \bar{X}_{N_2} \circ

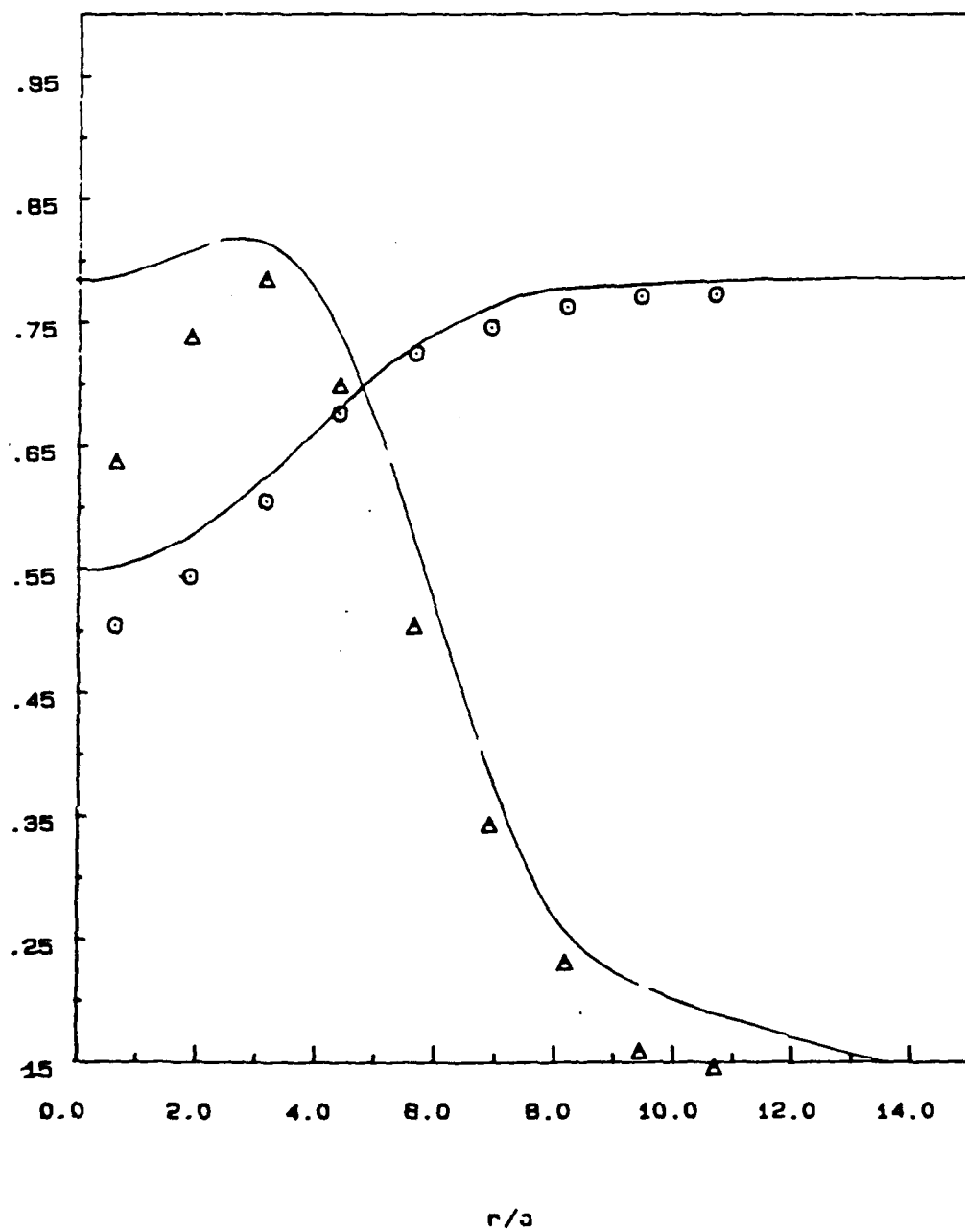


Fig. 6 Major species \bar{X}_1 at $x/d=25$; \circ \bar{X}_{H_2} , Δ \bar{X}_{CO} , \bar{X}_{CO_2} \square , \bar{X}_{O_2} +

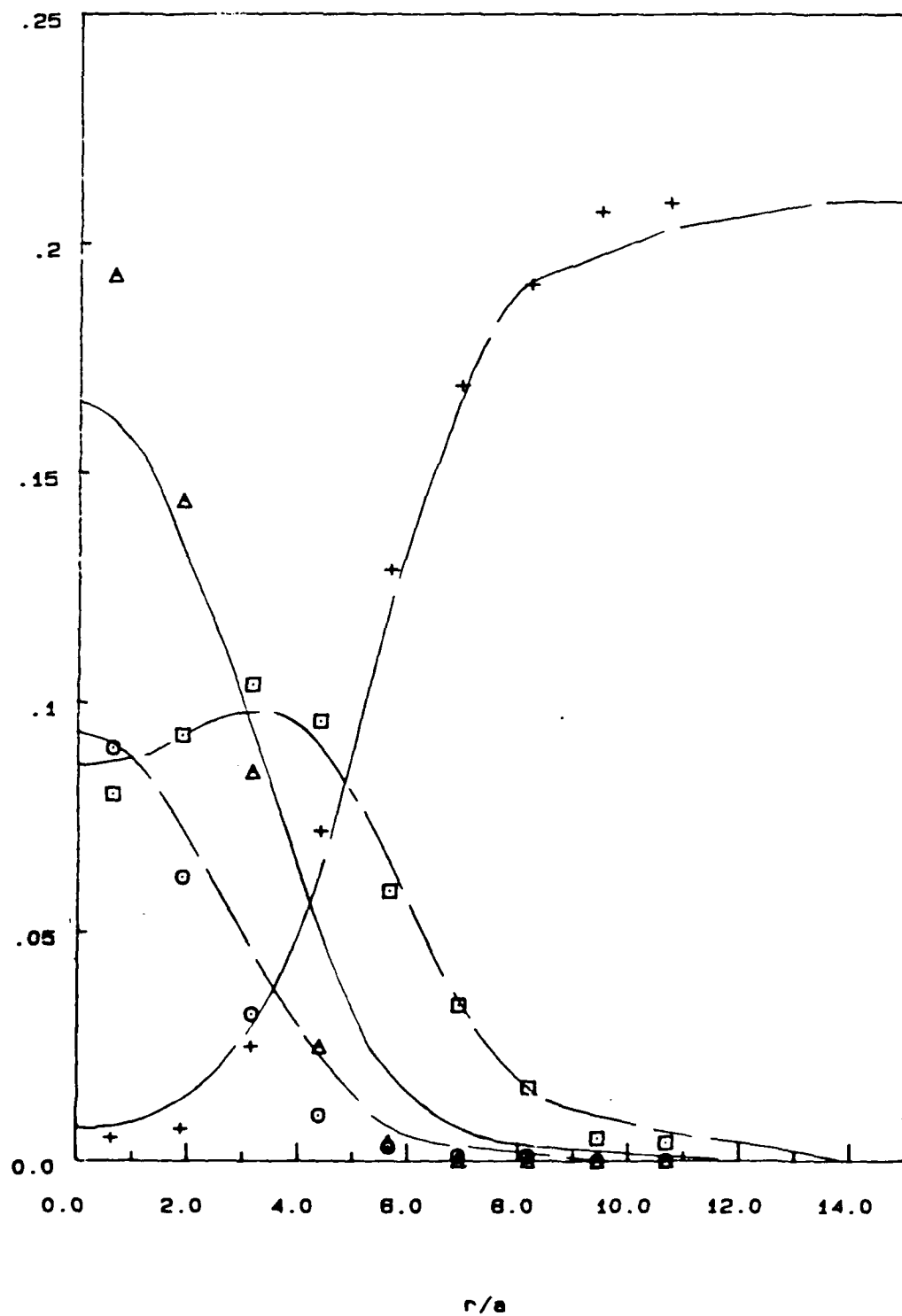


Fig. 7

Mixture fraction ξ and density $\bar{\rho}$ at $x/d=50$; ξ \square , $\bar{\rho}$ \circ

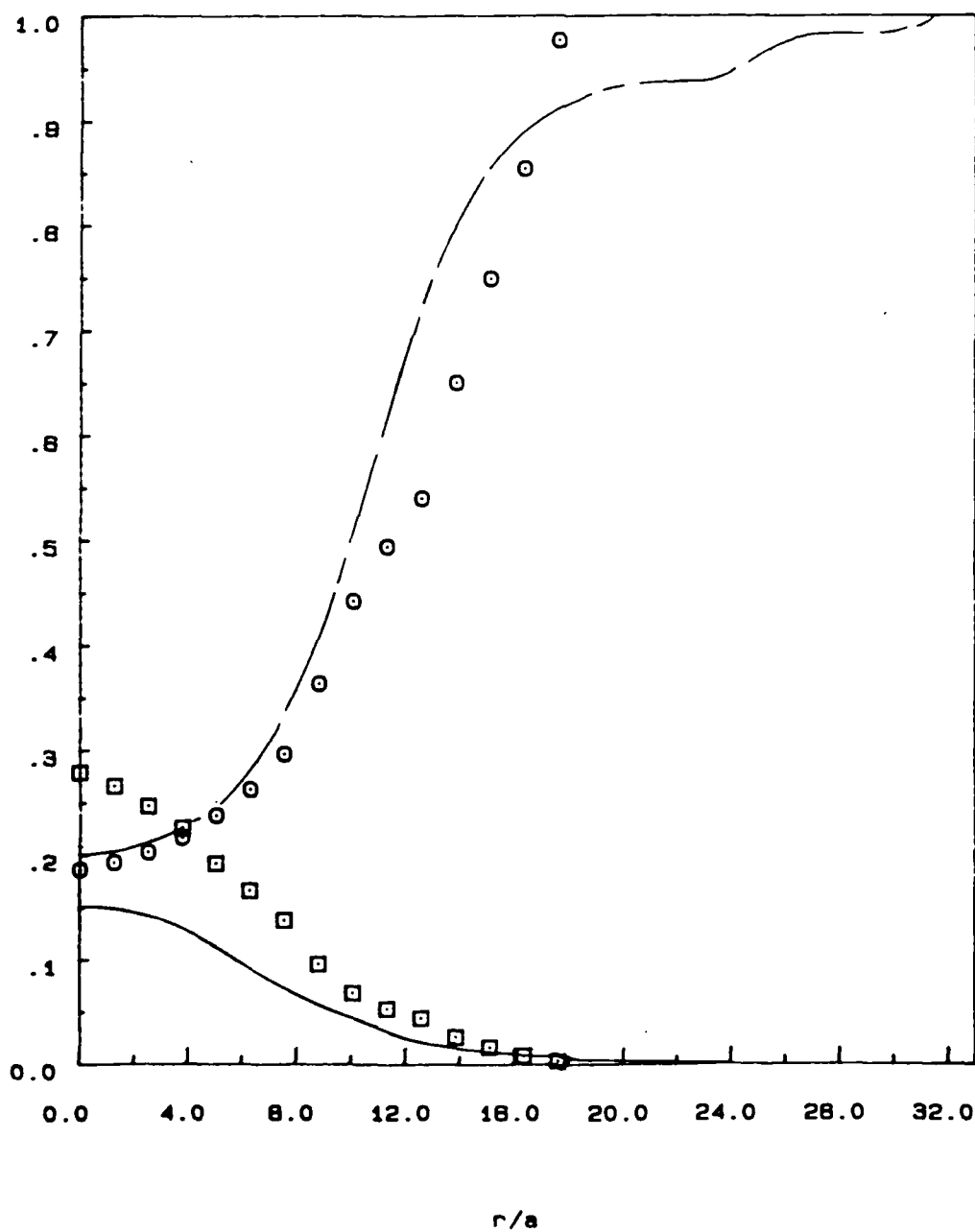


Fig. 8 Temperature \bar{T} and nitrogen mole-fraction \bar{X}_{N_2} at $x/d=50$; \bar{T} Δ , \bar{X}_{N_2} \circ

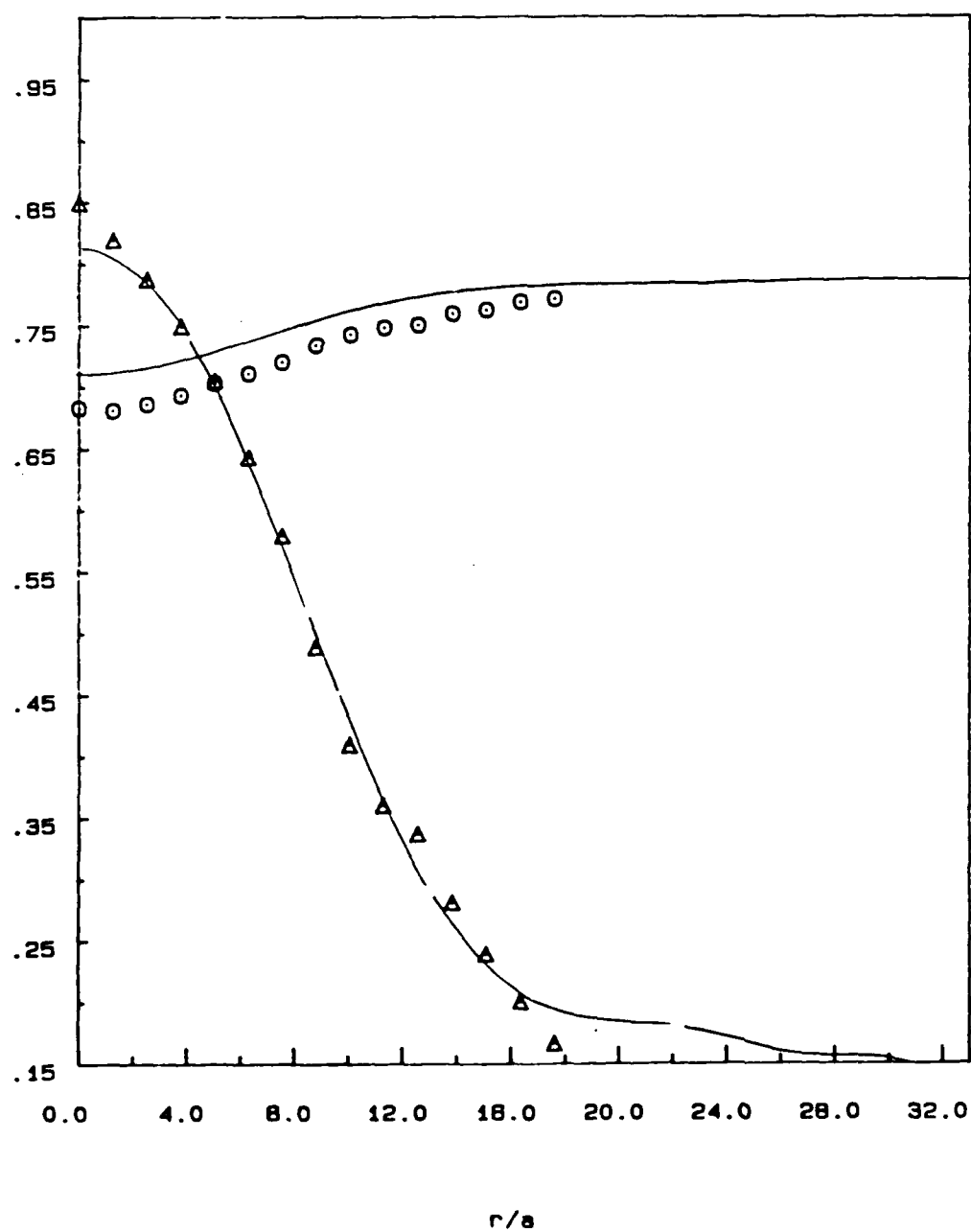
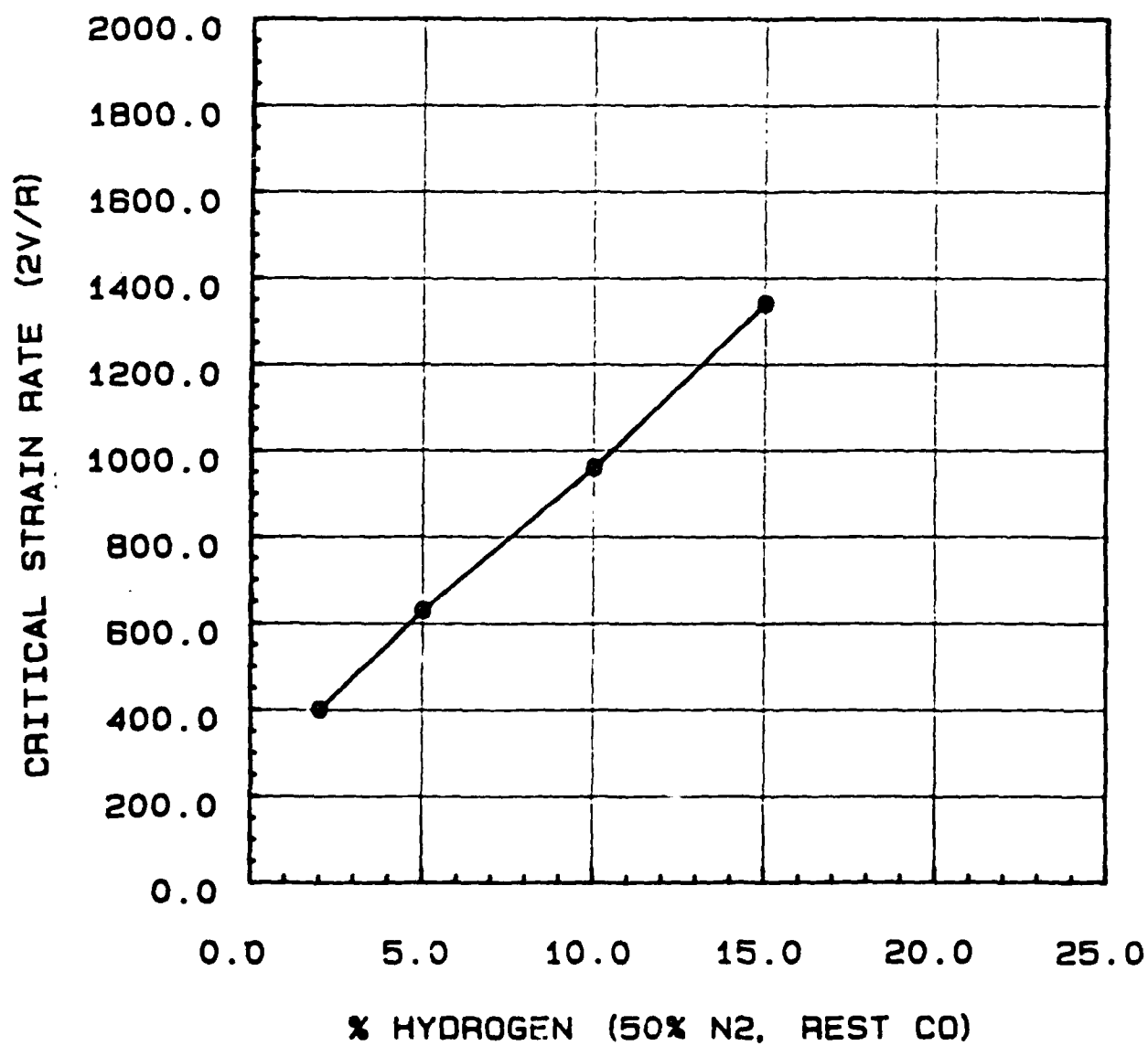


Fig. 9 Variation of α_c , the critical strain rate, with percent hydrogen in fuel (50% nitrogen, rest carbon monoxide).



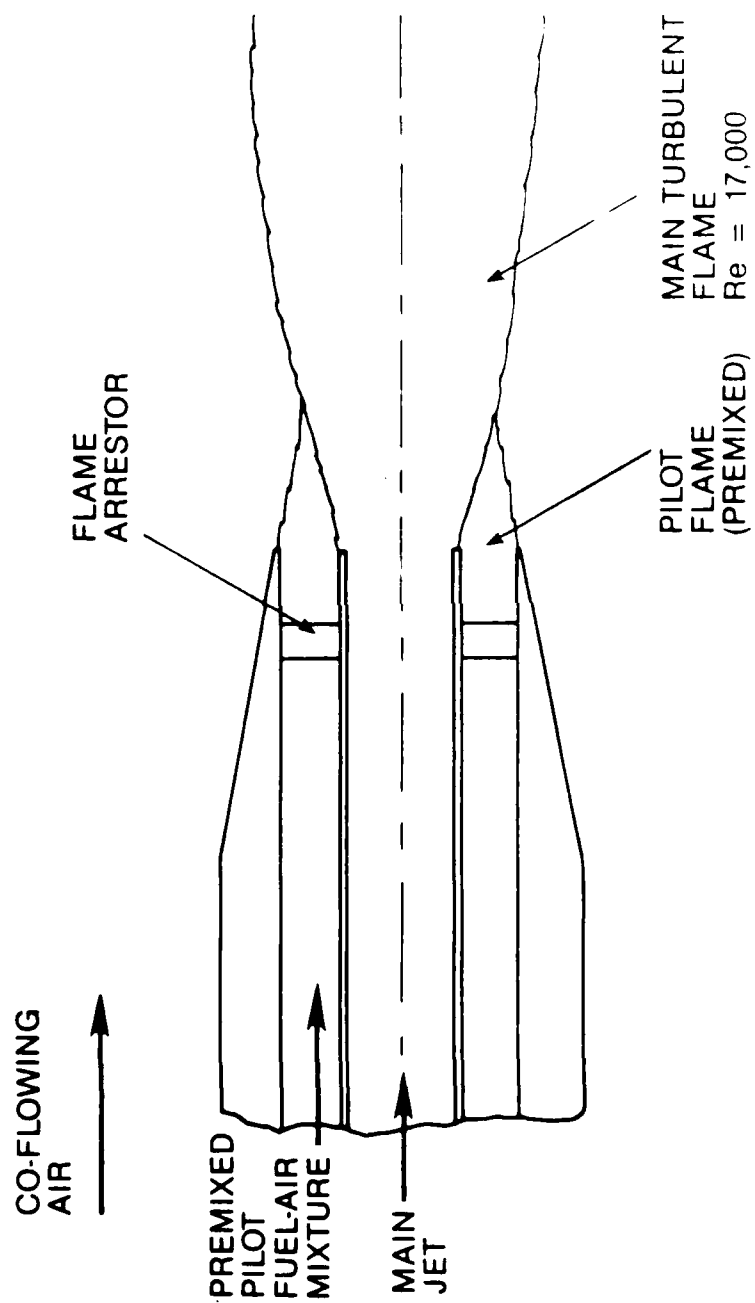


Fig. 10 Schematic of the burner exit.

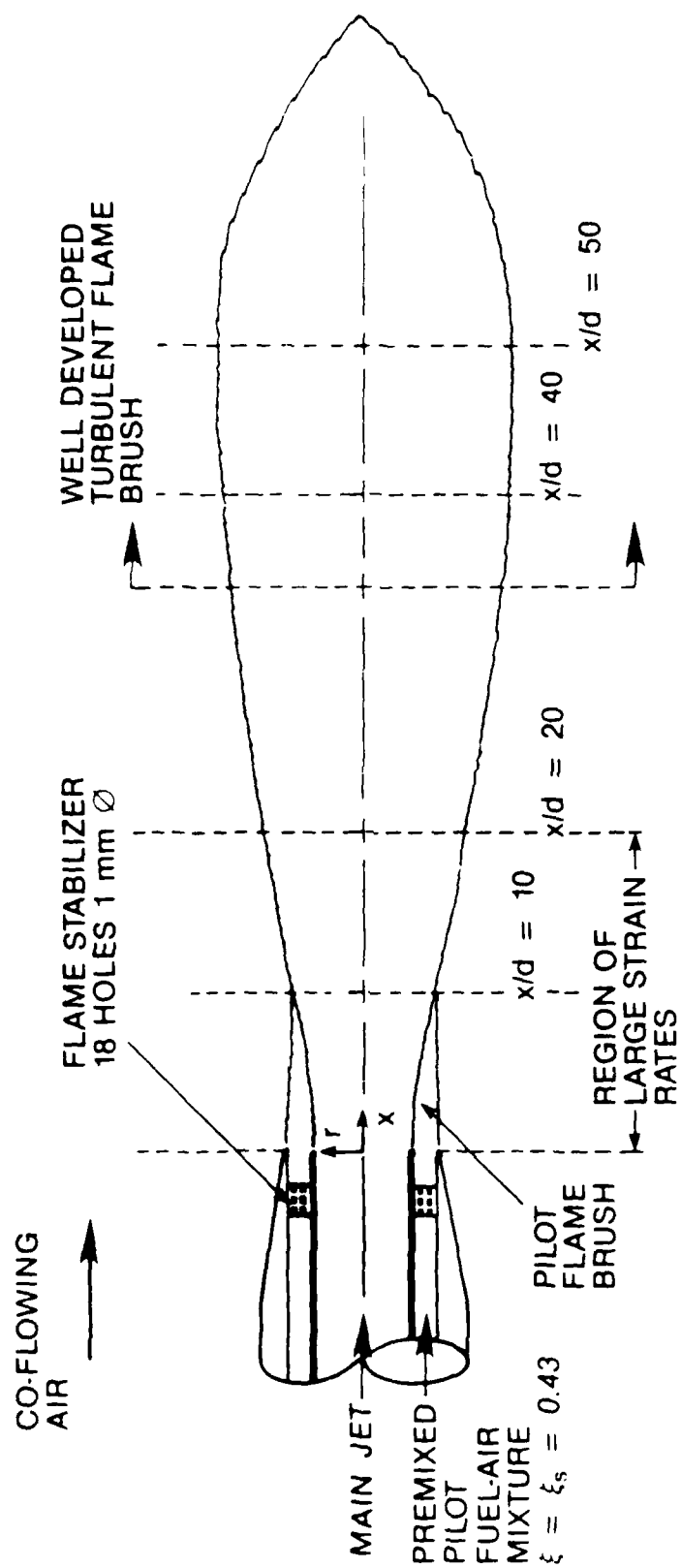


Fig. 11 Schematic of premixed pilot-stabilized burner showing the regions of maximum strain rates and fully developed turbulent-flame brush.

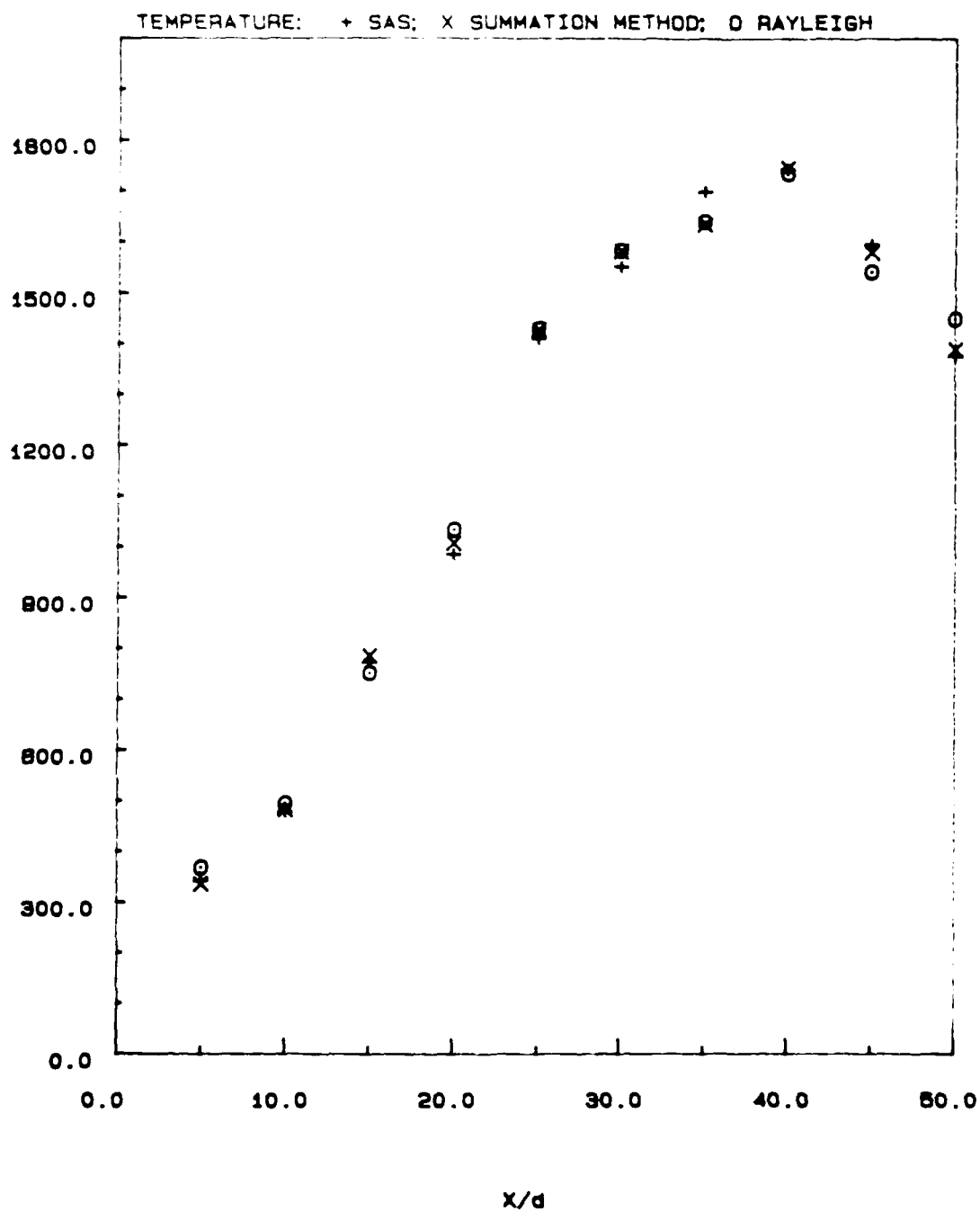


Fig. 12 Centerline axial profile of mean temperature in Re=15,000 flame using these methods (a) SAS, (b) sum of mole species and (c) Rayleigh scattering.

Fig. 13

Temperature vs. mixture fraction scattergram measured in the $Re = 5000$ flame at $x/d = 20$, $r/a = 2.52$ the solid line represents adiabatic equilibrium calculations for LHC gas in Figs. 13 through 15.

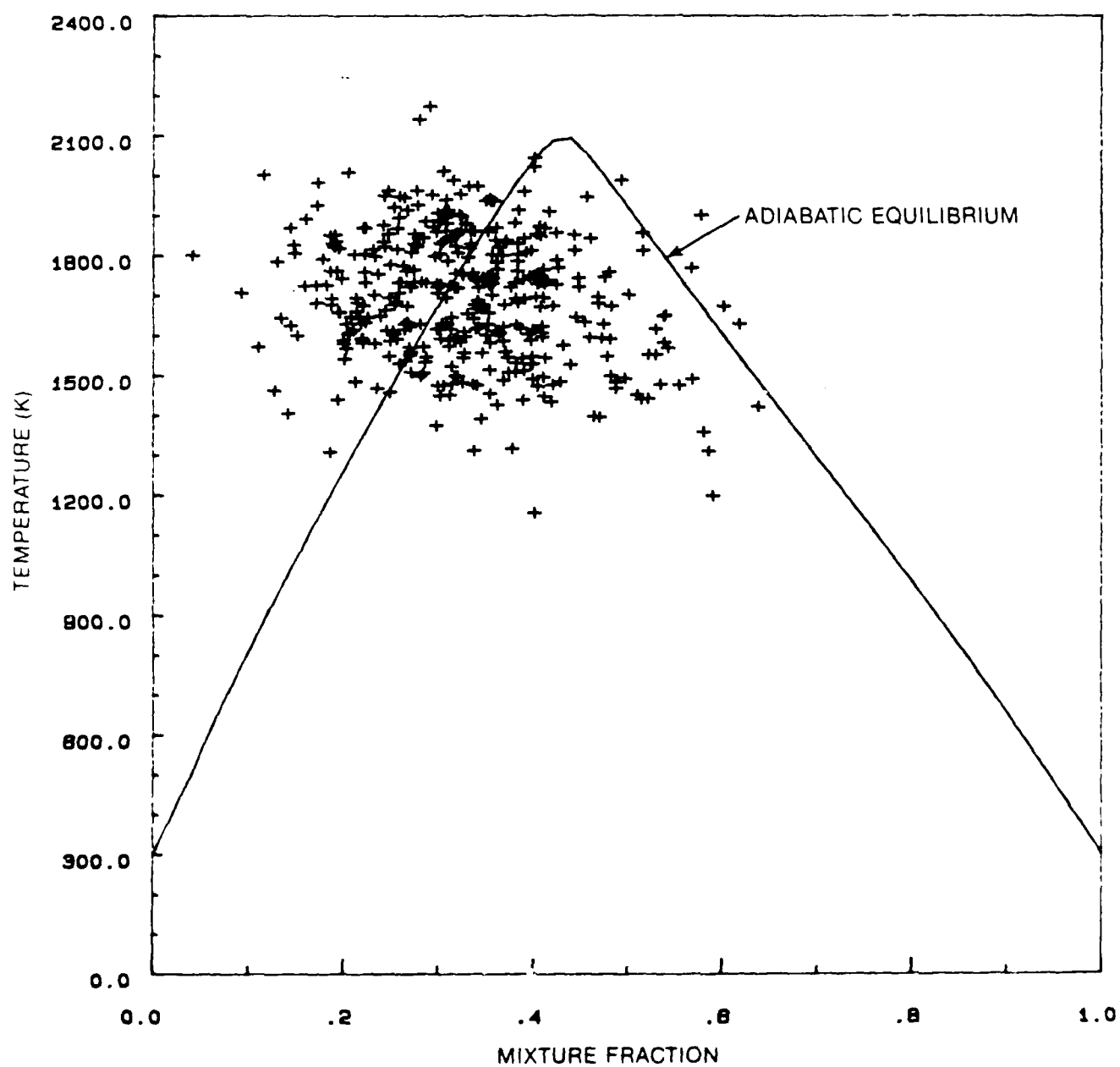


Fig. 14 Measured temperature vs. mixture fraction scattergram in the $Re = 15,000$ LHC flame at $x/d = 10$, $r/a = 1.89$.

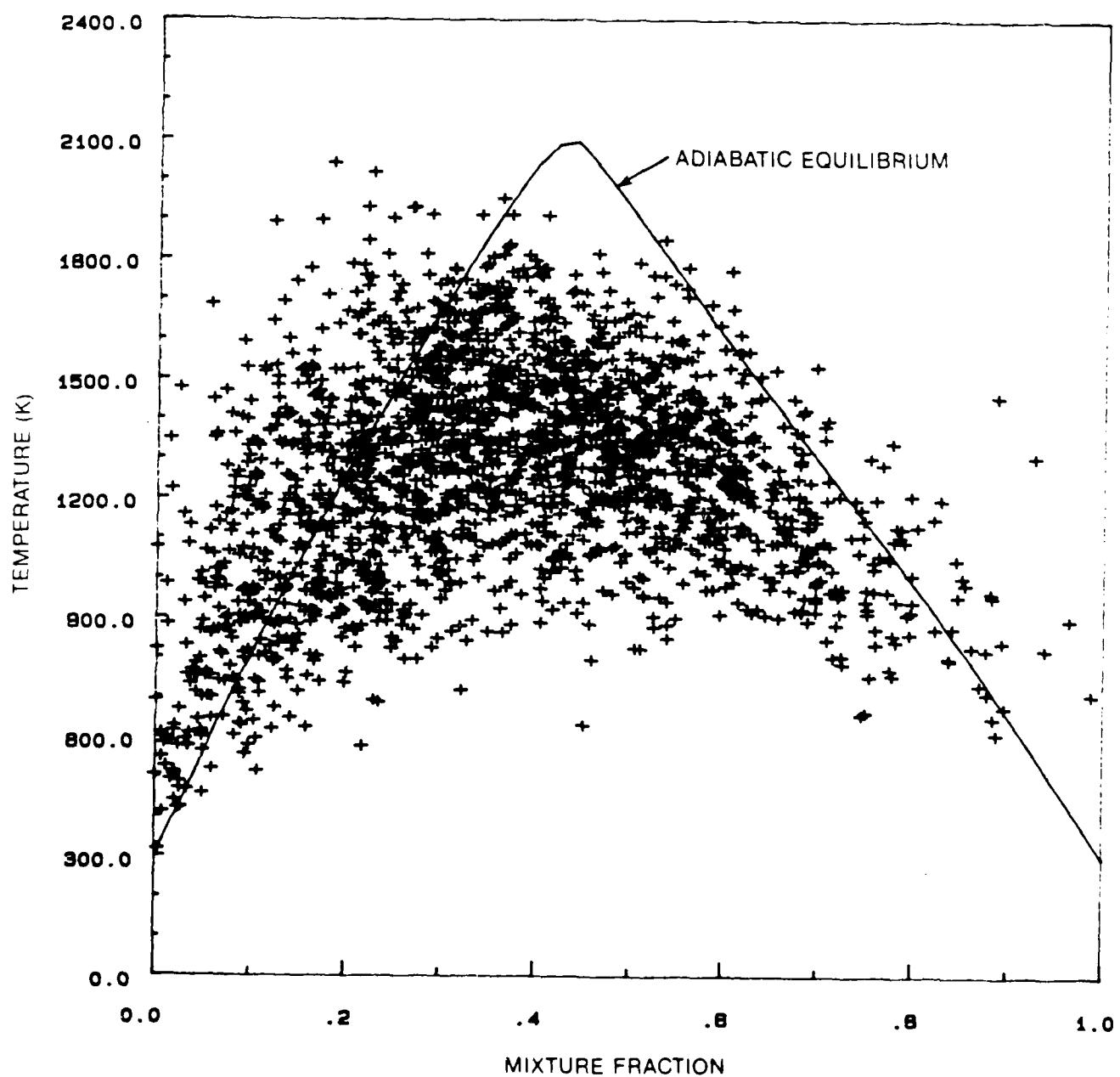
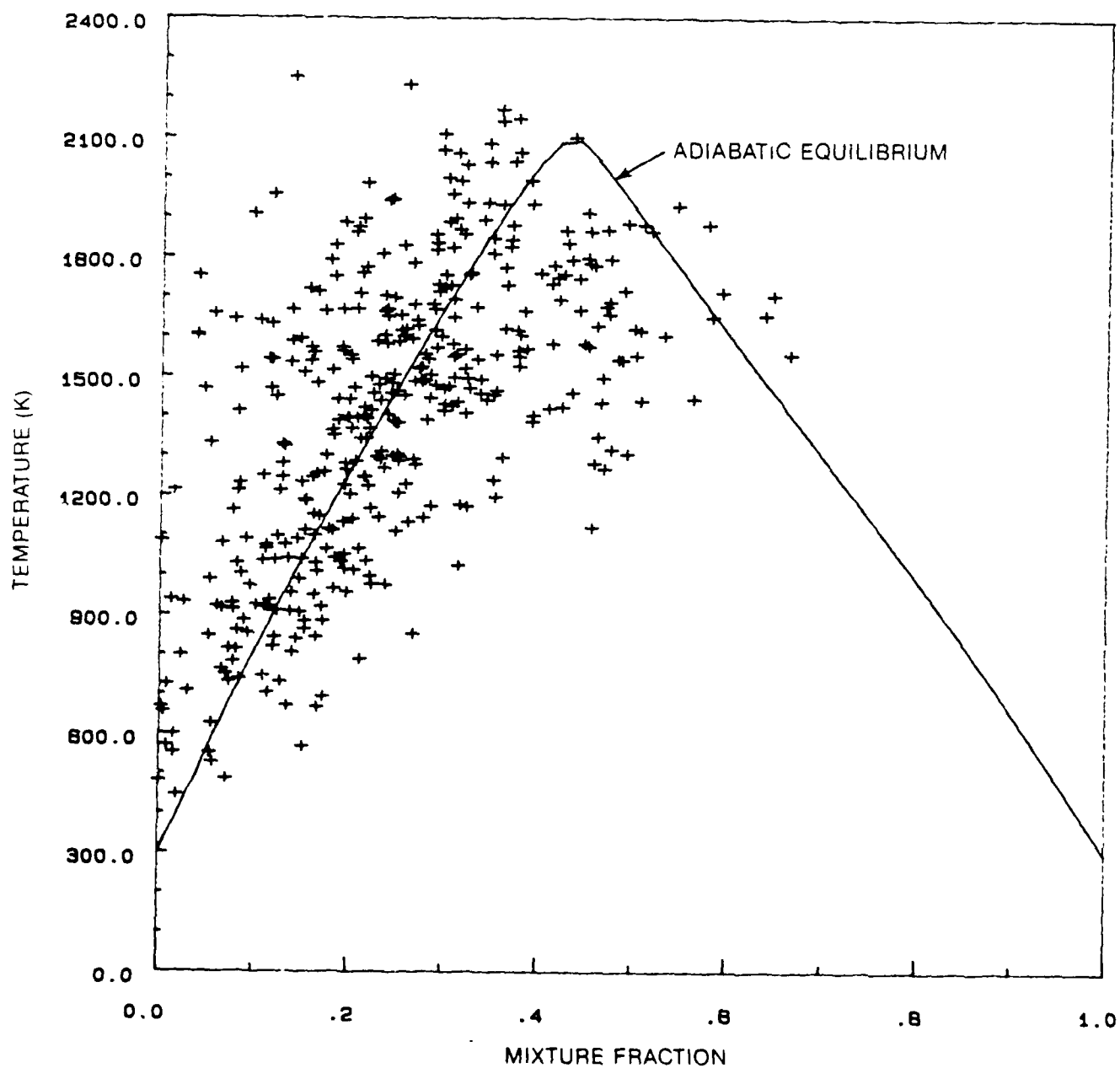


Fig. 15 Measured temperature vs. mixture fraction scattergram in the $Re = 15,000$ LHC flame at $x/d = 40$, $r/a = 3.77$.



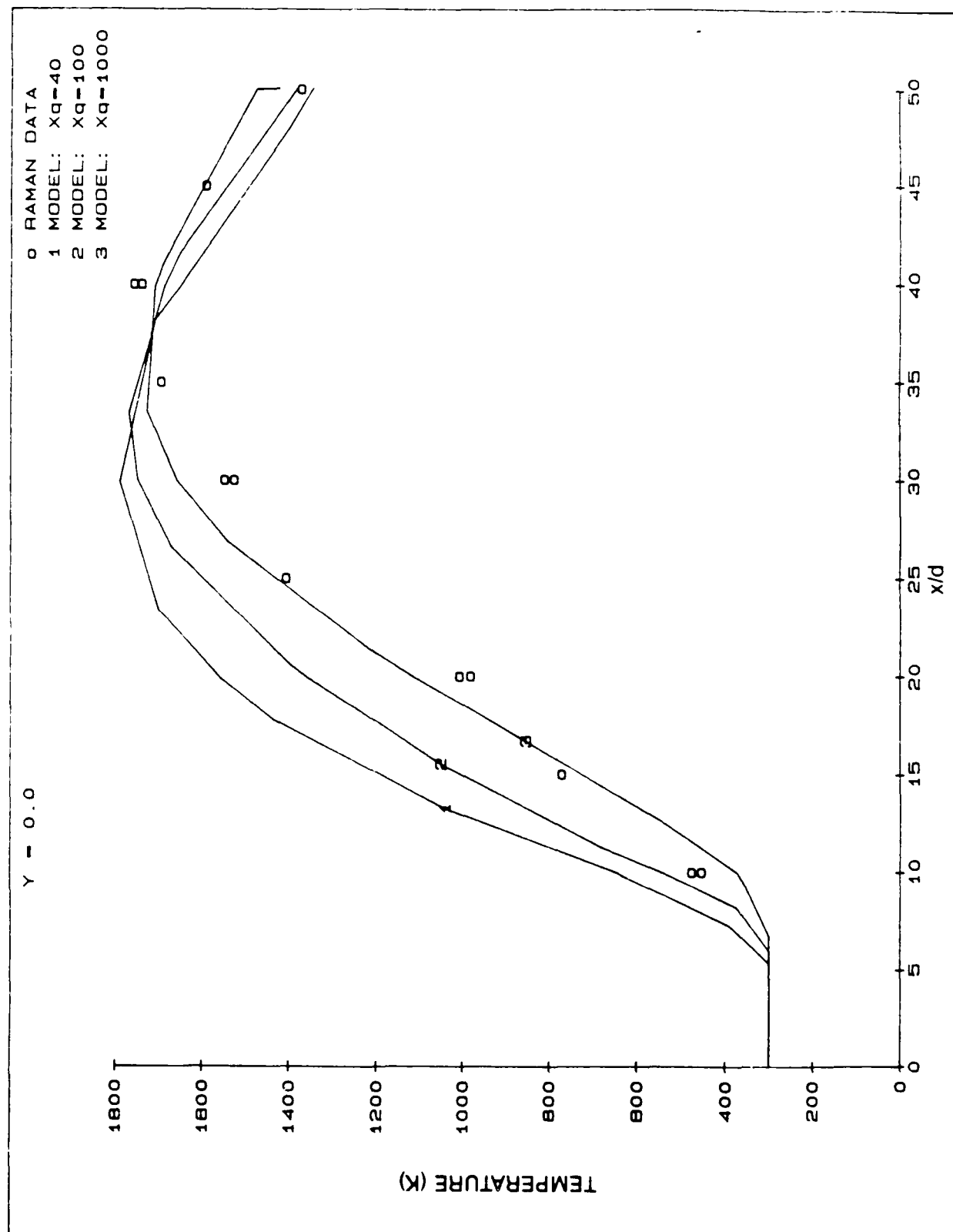


Fig. 16

Axial variation of mean temperature at $y = 0$ in the $Re = 15,000$ LHC flame. Model predictions for X_q of 40, 100 and $1000 s^{-1}$ are also shown in the figure.

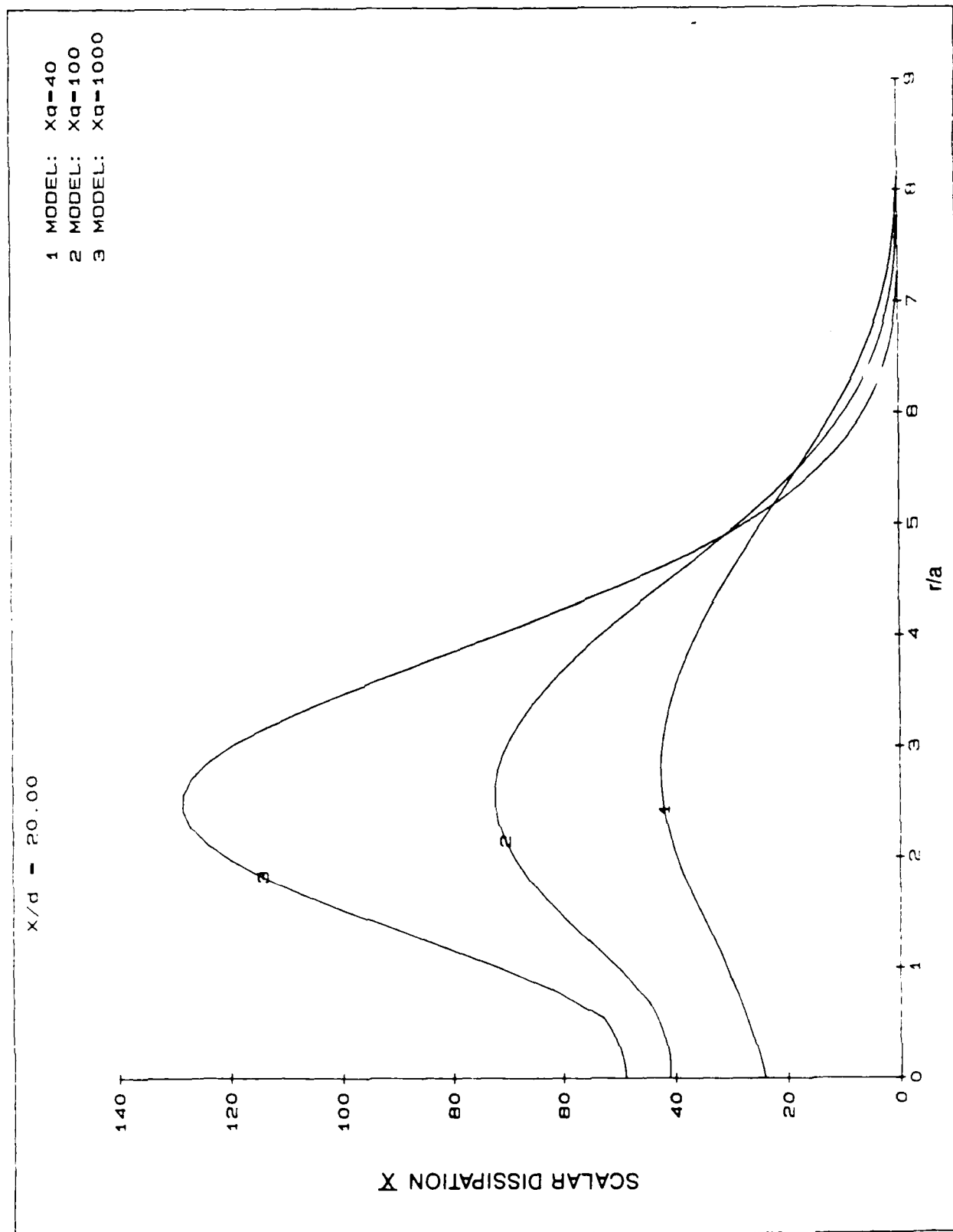


Fig. 17

Radial profile of predicted scalar dissipation rate of Liew et al. (1984). Stretched flamelet model at $x/d = 20$ for the values of $X_q = 40, 100$ and 1000 .

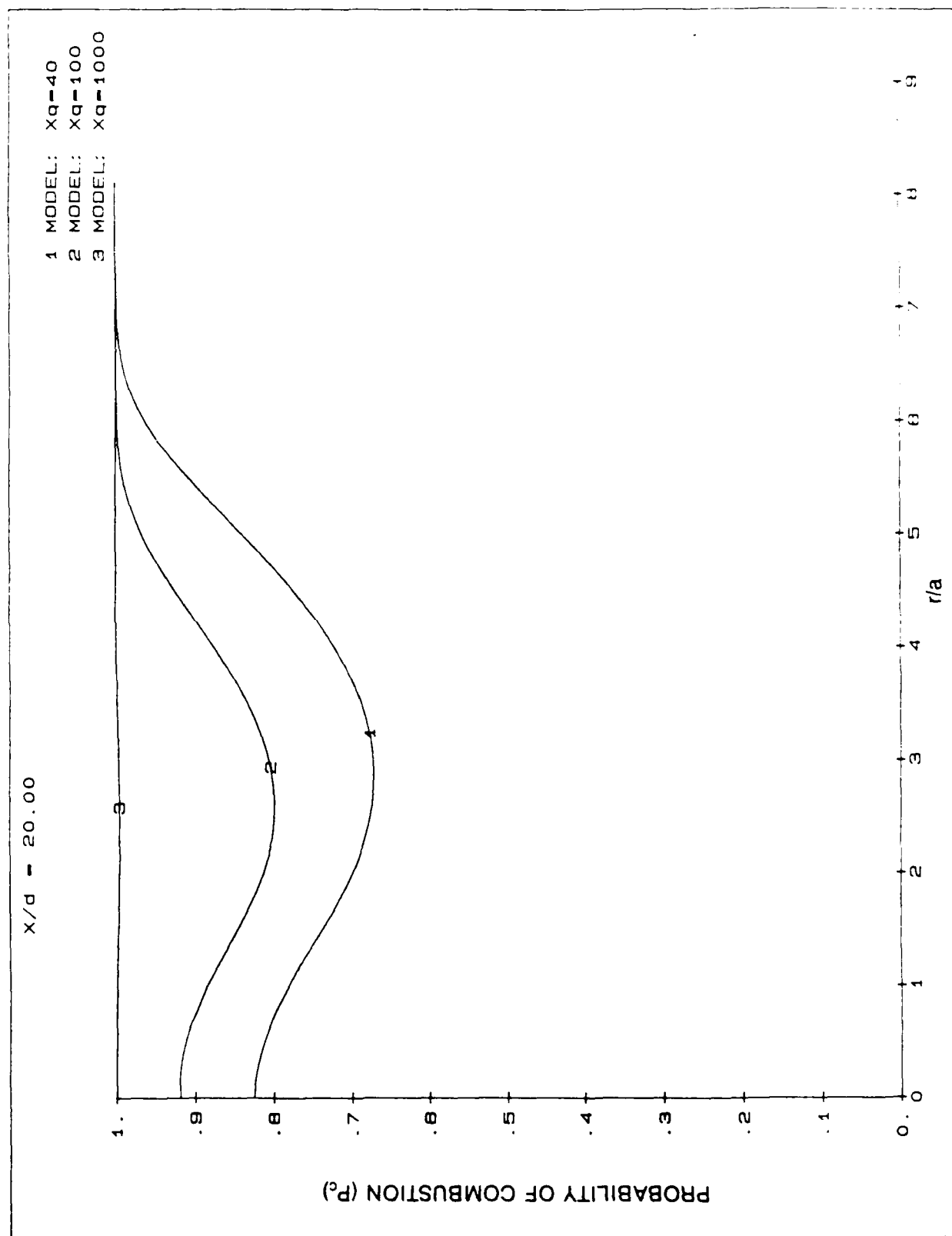


Fig. 18

Radial profile of predicted probability of combustion based on stretched flamelet model at $x/d = 20$ for three values of X_q .

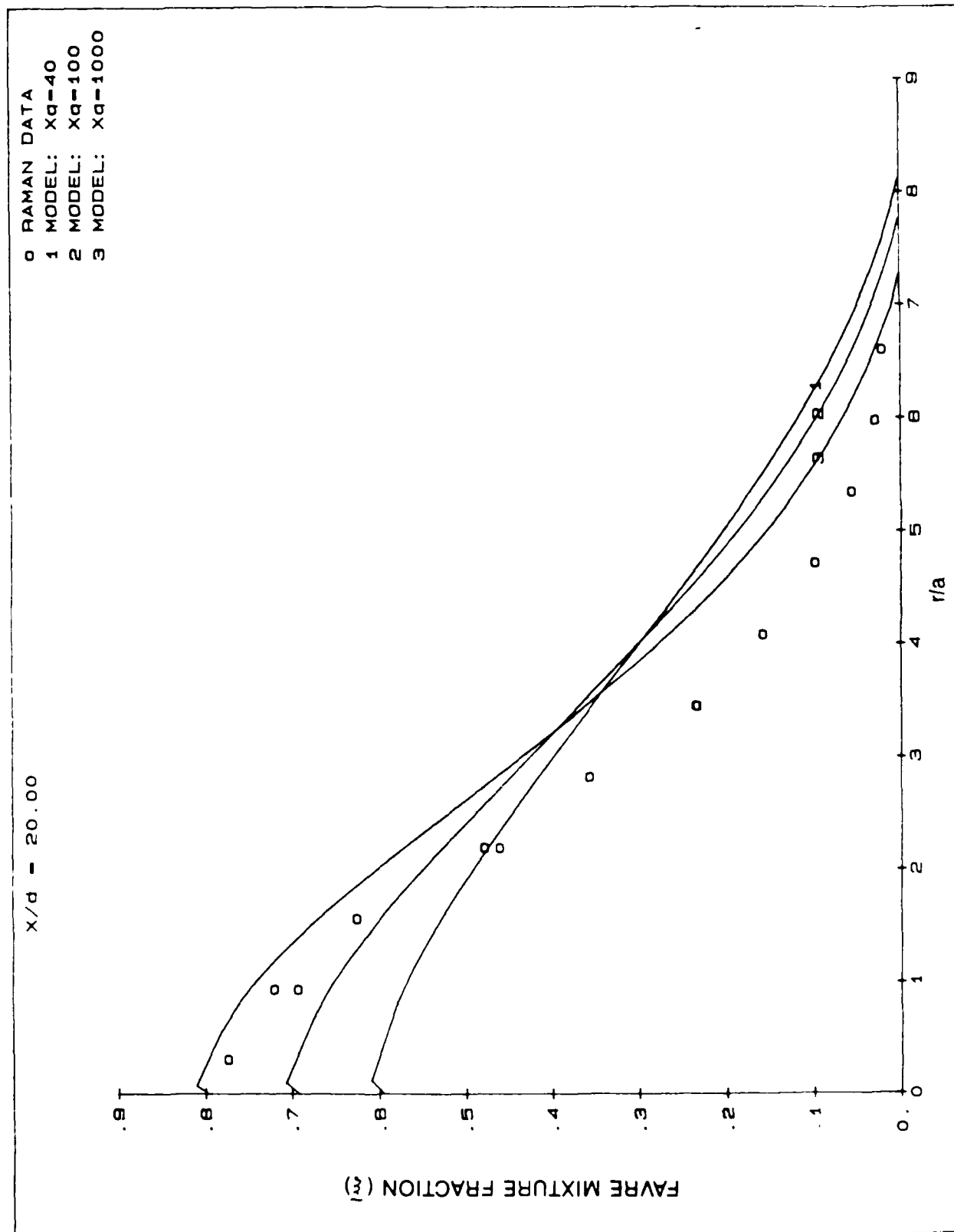


Fig. 19

Radial profile of measured Favre averaged mixture fraction at $x/d = 20$ compared with predictions of model for three values of X_q .

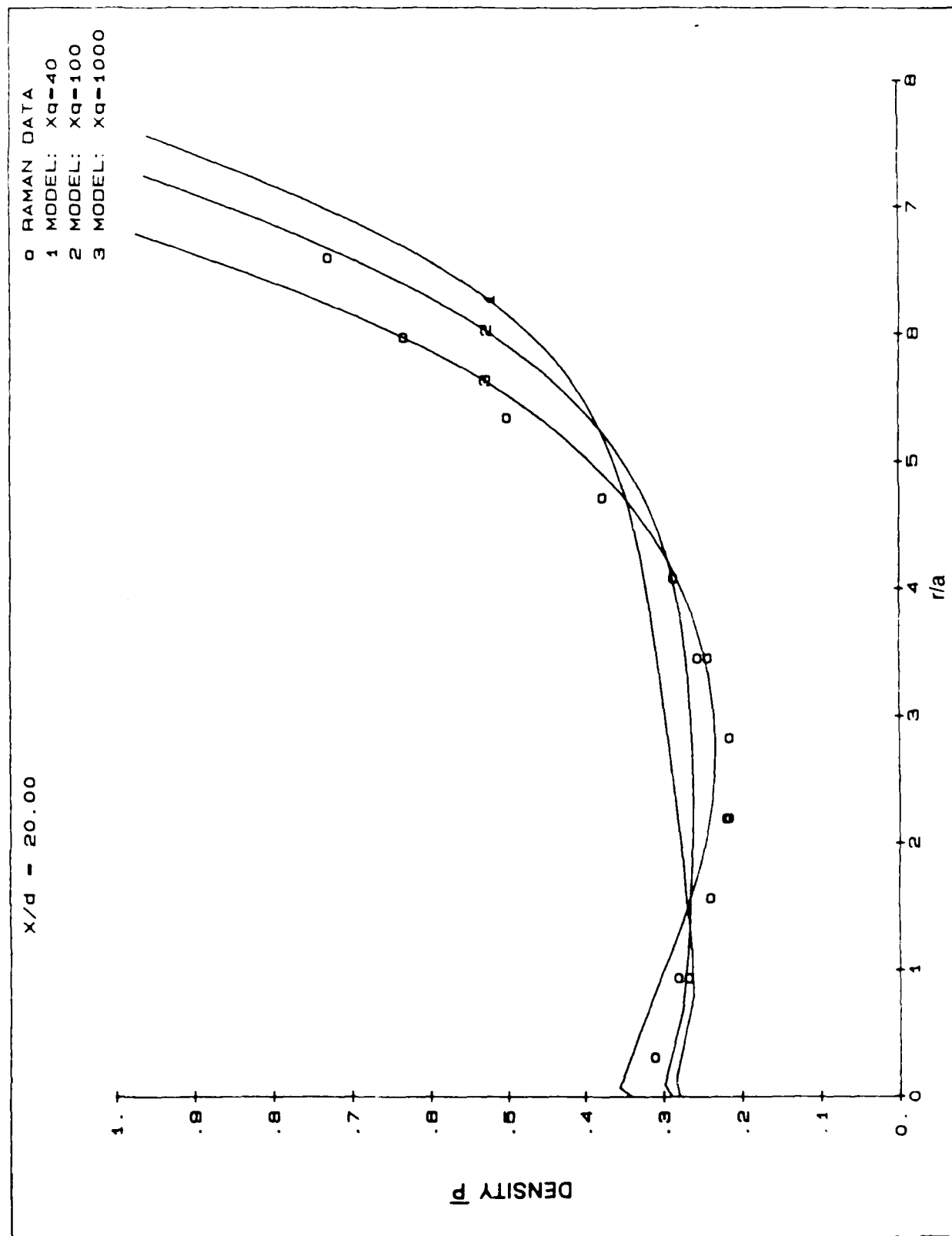


Fig. 20

Radial profile of measured mean density at $x/d = 20$ compared with predictions of model.

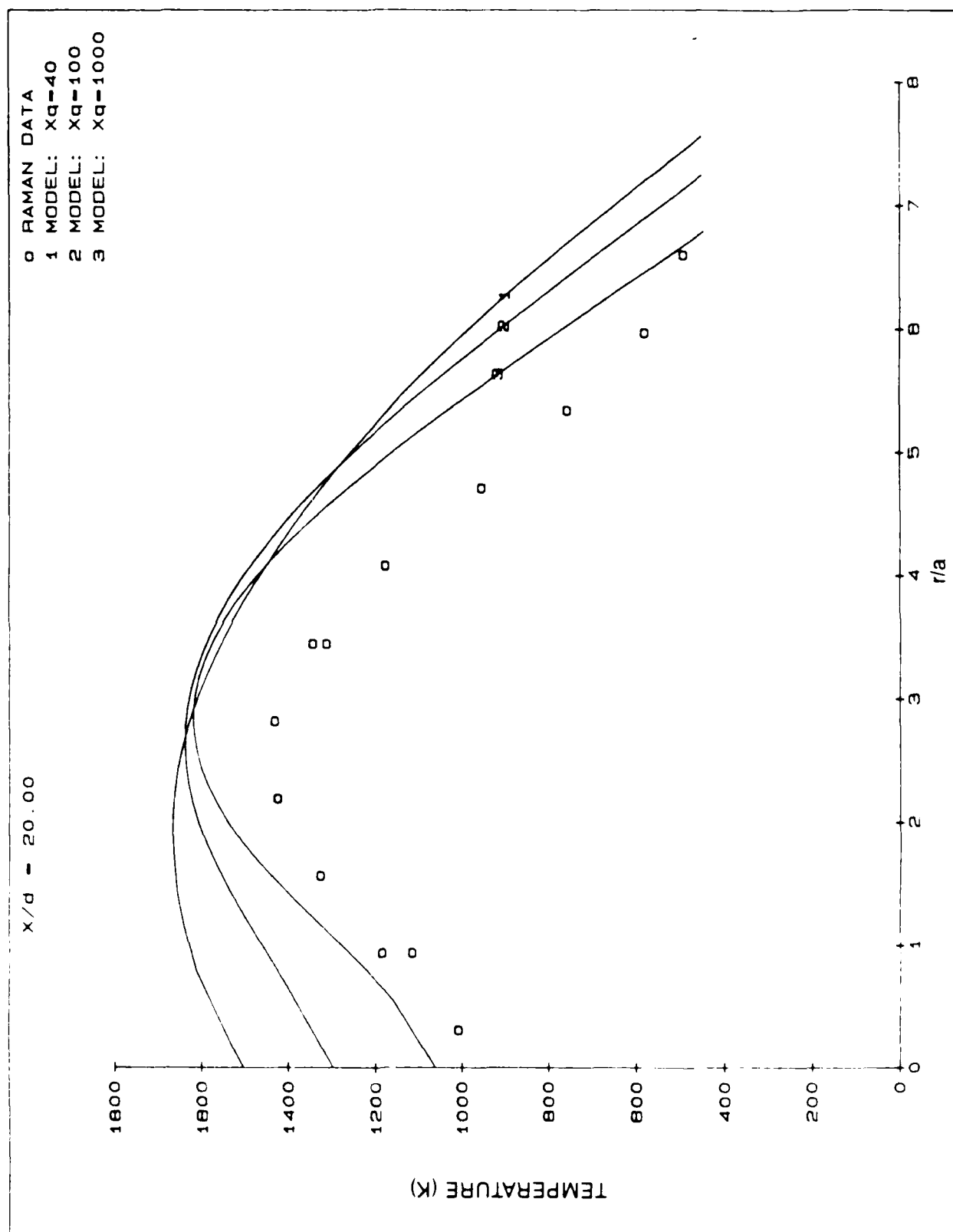


Fig. 21 Radial profile of measured mean temperature at $x/d = 20$ compared with predictions of model.

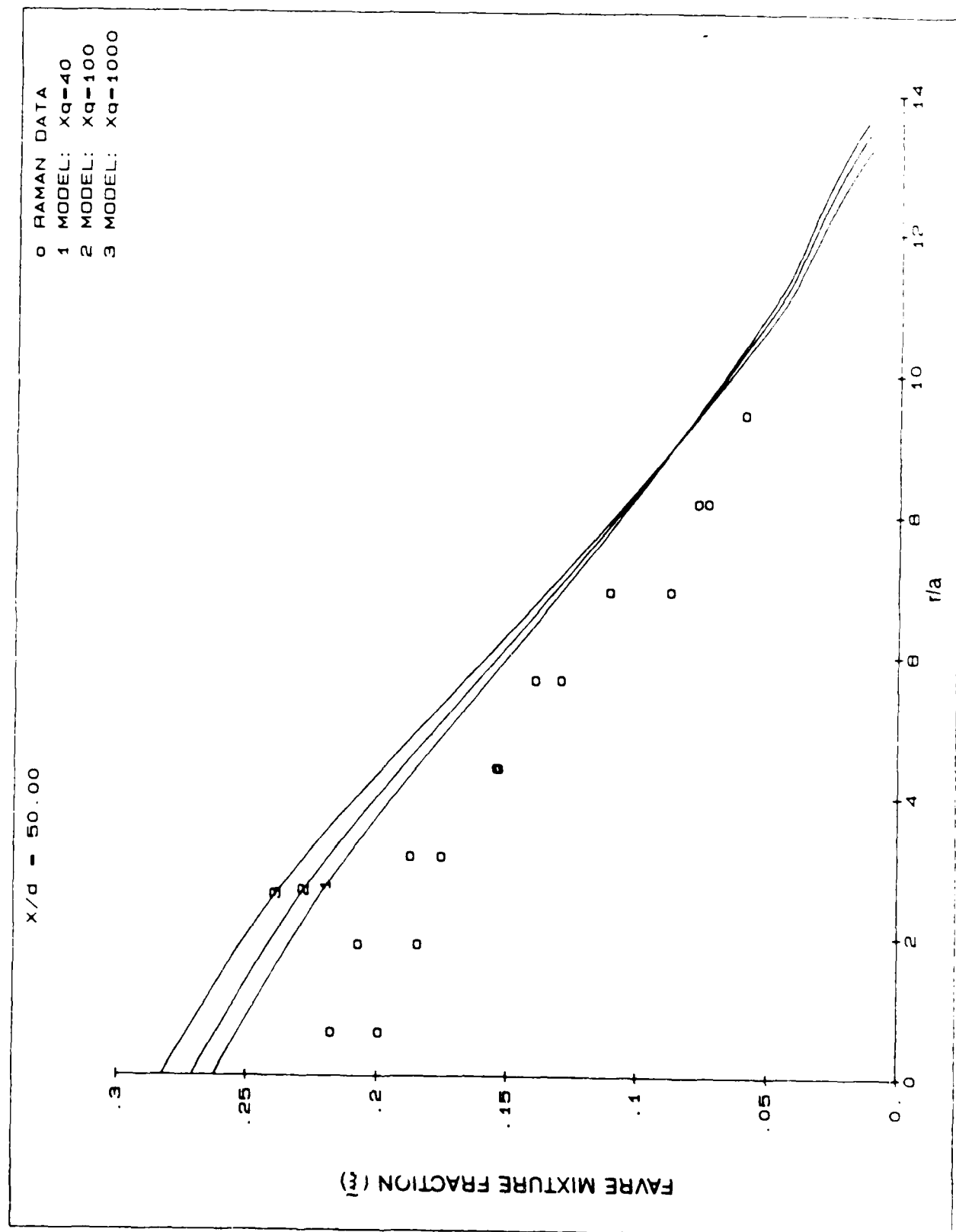


Fig. 22

Radial profile of measured Favre averaged mixture fraction at $x/d = 50$ compared with predictions of model.

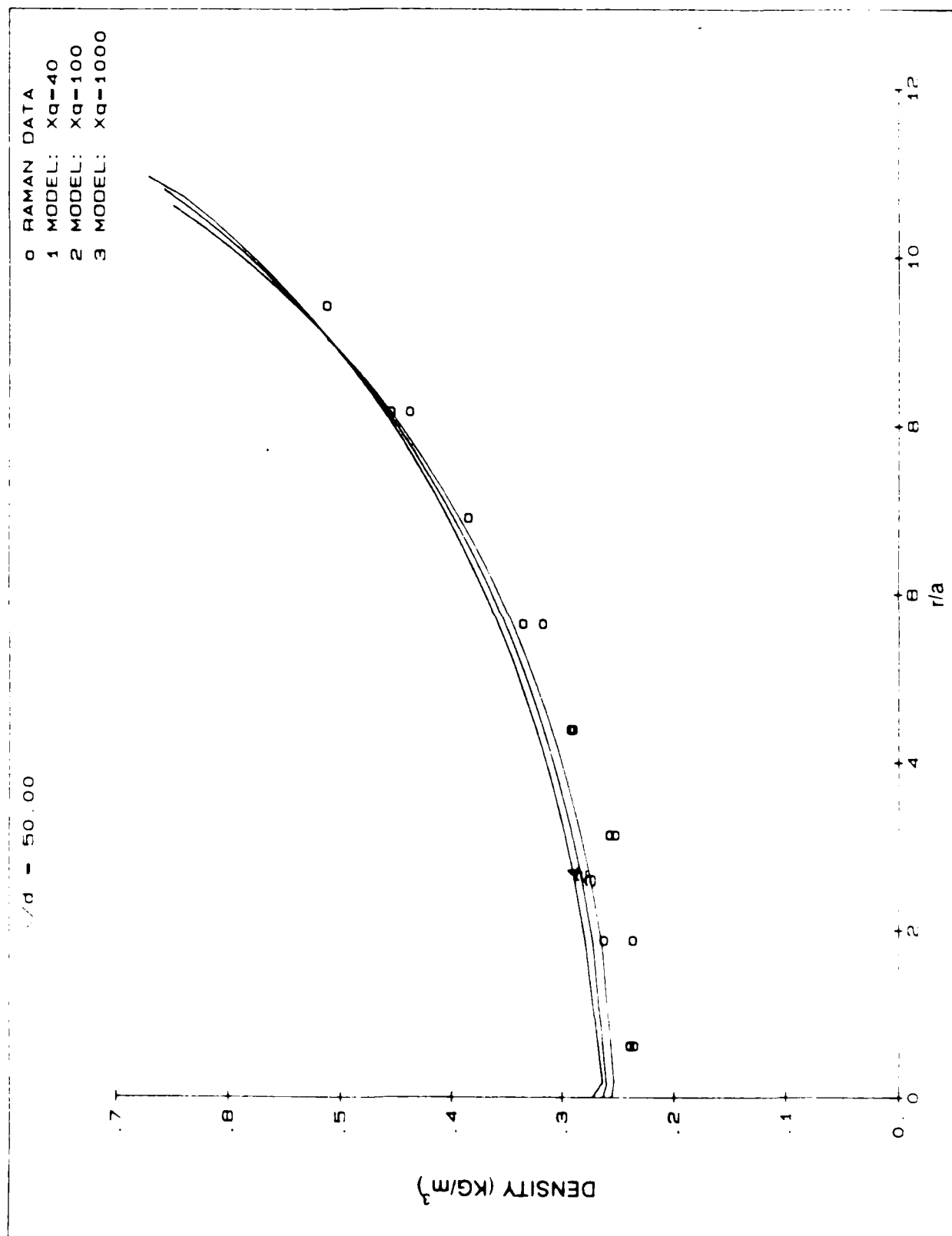


Fig. 23

Radial profile of measured mean density at $x/d = 50$ compared with predictions of model.

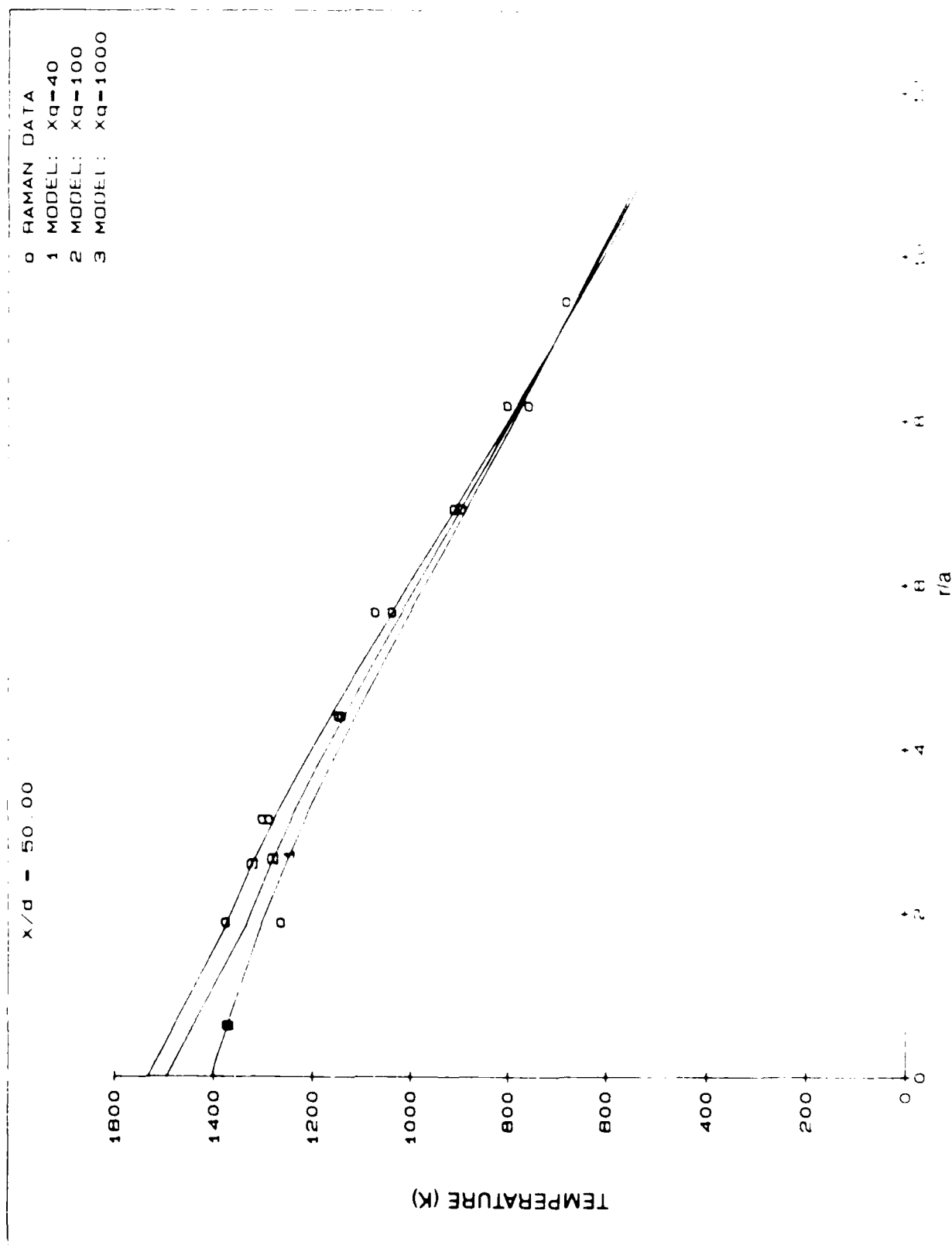


Fig. 24

Radial profile of measured mean temperature at $x/d = 50$ compared with predictions of model.

END

DATE

FILMED

DEC.

1987